CCAMLR

Commission for the Conservation of Antarctic Marine Living Resources
Commission pour la conservation de la faune et la flore marines de l'Antarctique
Комиссия по сохранению морских живых ресурсов Антарктики
Comisión para la Conservación de los Recursos Vivos Marinos Antárticos

WG-FSA-2025/37

20 September 2025

Original: English

WG-FSA

Spatial and environmental factors associated with Patagonian toothfish (Dissostichus eleginoides) distribution at South Georgia and the South Sandwich Islands (Subareas 48.3 & 48.4)

Jones, T., R.D. Cavanagh, S.E. Thorpe, T. Earl, J.J. Freer, S.L. Hill, C.M. Waluda, J. Cleeland, O.T. Hogg, P.R. Hollyman and M.A. Collins

EN

Spatial and environmental factors associated with Patagonian toothfish (*Dissostichus eleginoides*) distribution at South Georgia and the South Sandwich Islands (Subareas 48.3 & 48.4)

*T. Jones[1], *R. D. Cavanagh[1], S. E. Thorpe[1], T. Earl[2], J. J. Freer[1], S. L. Hill[1], Claire M. Waluda[1], J. Cleeland, O. T. Hogg[2], P. R. Hollyman[3] and M. A. Collins[1]

*Joint first authors
[1]British Antarctic Survey, NERC, Cambridge, UK
[2]Centre of Environment Fisheries and Aquaculture Science (Cefas), Lowestoft, UK
[3]School of Ocean Sciences, Bangor University, Askew Street, Menai Bridge, LL59 5AB, UK

Abstract

Understanding the environmental factors that drive the distribution of harvested fish species is essential for fisheries management, particularly in the context of climate change. Here, we investigated the spatial distribution of Patagonian toothfish (*Dissostichus eleginoides*) around South Georgia (Subarea 48.3) and the South Sandwich Islands (Subarea 48.4) in the southwest Atlantic sector of the Southern Ocean. Using scientific demersal trawl survey data, we identified and explored environmental factors linked to spatial distribution of juvenile to sub-adult Patagonian toothfish at South Georgia, with an emphasis on temperature and ontogenetic shifts. These findings were combined with an assessment of adult distribution across South Georgia and the South Sandwich Islands using longline fishery data. Trawl survey data collected at South Georgia were used to fit distribution models, informed by environmental covariates, for six different size-classes (total length: < 26 cm to > 66 cm) of Patagonian toothfish selected to approximately represent annual age groups. These were indicative of strong relationships with depth and temperature, with larger size-classes occupying progressively deeper habitats. Temperature effects were evident across all size-classes but were strongest for the three smallest size-classes, with higher abundances predicted at locations with annual mean sea surface temperature (SST) > 1.8°C. This suggests that spatial distribution patterns are

initially structured by surface or near surface temperatures for the smallest size-classes, patterns which are maintained throughout the first 3-4 years of growth. Fishery-derived data from the South Sandwich Islands, limited to toothfish available to the fishery within the depth range 700-2000 m, showed a step-like transition in catch-per-unit-effort (CPUE) in relation to seafloor temperature, with CPUE declining to near zero at or below 0.2-0.3°C, generally limiting their distribution to the northern part of the island chain. This study contributes to the work of WG-FSA in relation to understanding the drivers of spatial distribution across size-classes and life-history stages, including progressing recommendations from the CCAMLR Workshop on Climate Change. Our analyses of the complementary datasets confirm a strong influence of depth and temperature on Patagonian toothfish distribution, while providing new insight into the timing and nature of ontogenetic shifts and the environmental thresholds shaping spatial patterns. Understanding life stage-specific environmental sensitivities is important for improving forecasts of distributional shifts and informing ecosystem-based fisheries management in the context of climate change.

Introduction

The spatial distribution of marine fish is strongly influenced by environmental factors, including temperature and biogeographic boundaries (Pinsky et al., 2013), that define the conditions suitable for different species. These may vary according to age (Collin et al., 2021), maturity status (Bansemer and Bennett, 2011) and body size (Collins et al., 2005; Barbeaux and Hollowed, 2018). Many fish species occupy a specific thermal range determined predominantly by physiological limits (Portner et al., 2007; Ern et al., 2023) and modified by ecological or behavioural mechanisms (Beaugrand and Reid, 2003; Neubauer and Andersen, 2019). High-latitude fish, for example, can be restricted by cold water boundaries and may face habitat loss as temperatures rise (Dulvy et al., 2008; Thorson, 2019). In addition, deep and cold boundary zones can act as refuges or limits, influencing where species can successfully survive, grow and reproduce (Mueter and Litzow, 2008; Hollowed et al., 2012; Aschan et al., 2013; Sandersfeld et al., 2017).

Understanding the environmental factors that drive the distribution of target species is essential for fisheries management, and increasingly so in the context of climate change. Climate-driven shifts in fish distributions may lead to population declines in some areas, while in others, species may expand or be displaced from their usual ranges, presenting challenges for management (Sunday et al., 2012; Cavole et al., 2016; Melbourne-Thomas et al., 2022; Townhill et al., 2023). These include disruption to fishery-related scientific surveys, changing stock dynamics and issues for international management bodies (Azmi et al., 2025; Barange et al., 2018; Cruz et al., 2024; Bessell-Browne et al., 2025).

Here we focus on Patagonian toothfish (*Dissostichus eleginoides* Smitt 1898), a commercially fished notothenioid with a circumpolar distribution around islands and continental shelves in the Southern Ocean and South Atlantic, including South Georgia (Subarea 48.3) and the South Sandwich Islands (SSI; Subarea 48.4), the focal region for this study (**Figure 1**). The Patagonian toothfish population at South Georgia, Shag Rocks, and the northern SSI, is considered a largely self-contained stock, with limited connectivity to other populations, and lies at the southern limit of the species' range (Shaw et al., 2004; Collins et al., 2010; Rogers et al., 2006; Soeffker et al., 2022). In the SSI, the southern distribution limit overlaps with the northern limit of Antarctic toothfish (*Dissostichus mawsoni* Norman, 1937*)*, with thermal gradients - reflecting underlying physiological differences between the species - structuring this transitional zone between sub-Antarctic and Antarctic waters (Roberts et al., 2011; Hollyman et al., 2022; Soeffker et al., 2022). While it is worth noting that Arkhipkin et al. (2022) proposed that stocks of *D. eleginoides* on the Patagonian Shelf and at South Georgia are sufficiently distinct to be considered separate species, this has yet to be verified and hence we continue to use *D. eleginoides* for both populations.

The archipelagos of South Georgia and the SSI are part of the Scotia Arc, a predominantly submarine ridge that forms the perimeter of the Scotia Sea. The region encompasses a broad-range of oceanographic conditions, transitioning from warmer sub-Antarctic conditions in the north to areas characterised by seasonal ice-cover in the south (Thorpe and Murphy, 2022; **Figure 1**). The South

Georgia and Shag Rocks shelves (average depth ≈ 200 m; Gregory et al., 2017) are separated by a deep canyon (maximum depth of 2000 m) and lie within the Antarctic Circumpolar Current (ACC), to the south of the Polar Front. Shag Rocks, located closer to the Polar Front, typically experiences warmer surface conditions than around South Georgia, which is influenced more strongly by the Southern ACC Front (SACCF) and cooler subpolar waters, as well as glacial run off (ref; **Figure 1**). The ACC and its frontal systems exhibit strong intra- and interannual variability which drives variability in the conditions experienced at Shag Rocks and South Georgia (Meredith et al., 2005, Murphy et al., 2007, Boehme et al., 2008, Combes et al., 2023). The SSI, the northernmost of which is c. 550 km from South Georgia, are small and volcanically active prominences of a submarine ridge at the eastern end of the Scotia Arc. Due to their steep topography, depth increases rapidly between the islands with deep water passages (> 1500 m at their deepest) running east to west at multiple locations along the SSI chain (**Figure 1**). The SACCF passes between South Georgia and the South Sandwich Islands, with the southern boundary of the ACC deflected north along the western side of the SSI. The region is undergoing rapid climate-driven changes, including in ocean temperature, winds, circulation, and sea ice extent and duration (Whitehouse et al., 1998; IPCC, 2019; 2022; Cavanagh et al., 2021; Hogg et al., 2021).

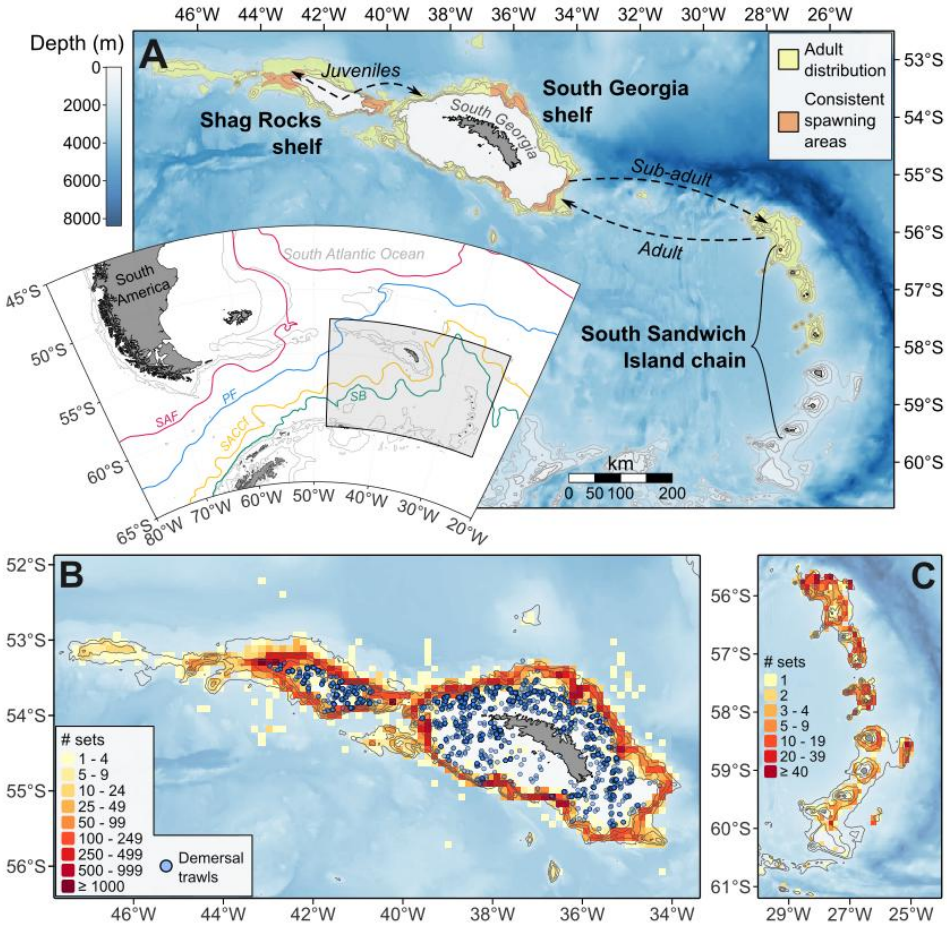

Figure 1. *Maps showing the location of the study region in the Atlantic Sector of the Southern Ocean in relation to South America and major oceanographic features (SAF = Subantarctic Front, PF = Polar Front, SACCF = Southern Antarctic Circumpolar Current Front, SB = Southern Boundary of Antarctic Circumpolar Current; Park and Durand 2019), with subsequent panels providing information on Patagonian toothfish (Dissostichus eleginoides) distribution and spatial ecology (**A**) and the distribution of data used in this study (**B** & **C**). The distribution of Patagonian toothfish in the study region (**A**) is shown with reference to the distribution of adults, consistent spawning grounds (Belchier and Collins, 2008; Bamford et al., 2024), and suspected ontogenetic movement between areas (Collins et al.,2010; Soeffker et al., 2022). Available data on Patagonian toothfish distribution and abundance is shown as the location of demersal trawls carried out during groundfish surveys (1987-2023) at South Georgia (**B**) and via the number of longline sets in the South Georgia (**B**) and South Sandwich Island (**C**) longline fisheries, shown as density heatmaps (number of lines set in 10×10 km grid-cells). Bathymetry data shown in each panel were sourced from the ETOPO 2022 (NOAA 2022) dataset, and contour lines represent the 500, 1000, 1500, and 2000 m isobaths.*

How Patagonian toothfish will be affected by these ongoing changes is uncertain (IPCC, 2019). The life history of this long-lived species (~50 years) includes a prolonged pelagic phase during early development. Eggs and larvae are planktonic in surface waters and therefore may be susceptible to

changes in SST, which may influence planktonic duration, development rate and survival of eggs and larvae (North, 2002). Following dispersal, larvae settle as small juveniles to demersal habitats in shallow waters with a gradual migration deeper as they grow (Collins et al., 2010). These ontogenetic shifts result in exposure to a range of environmental conditions throughout the species' development (Cavanagh et al., 2025). Retention of eggs and larvae near juvenile habitat at South Georgia and Shag Rocks is influenced by oceanographic conditions, with prevailing currents likely influencing juvenile recruitment (Brigden, 2019). The smallest post-settlement fish in this population (length < 20 cm) are found mainly on the continental shelf near Shag Rocks at depths of 100 - 300 m (Collins et al., 2007, 2010; Belchier and Collins, 2008), adopting a primarily benthic lifestyle, although smaller individuals may also forage in the water column (Collins et al., 2007). As individuals in this population grow, they gradually disperse to deeper water, spreading outward from their initial habitats (Collins et al., 2010). Spawning occurs annually in austral autumn and winter, typically along the South Georgia–Shag Rocks continental slope (Bamford et al., 2024; **Figure 1**), likely influenced by oceanographic conditions including temperature (Everson and Murray, 1999; Boucher, 2018; Brigden, 2017, 2019; Bamford et al., 2024). While there is evidence of all life-stages at South Georgia, there is no indication of spawning at the SSI, such that individuals occupying the northern portion of the SSI chain may result from spill-over from South Georgia following periods of high recruitment (Soeffker et al., 2022). The lack of antifreeze proteins in Patagonian toothfish (compared to their Antarctic congener *D. mawsoni*) may limit their polewards range (Collins et al., 2010; Roberts et al., 2011; Hollyman et al., 2022; Soeffker et al., 2022), with Eastman (1990) suggesting a lower temperature limit of 2°C, although individuals have since been observed at temperatures of 1.4°C (Collins et al., 2005).

Patagonian toothfish are the target species of a valuable deepwater commercial longline fishery that began in the late 1980s (Agnew, 2000; Collins et al., 2010). In South Georgia waters, the fishery is managed within the framework of the Commission for the Conservation of Antarctic Marine Living Resources (CCAMLR) (https://fisheryreports.ccamlr.org/). The stock assessment informing management of Patagonian toothfish at South Georgia and Shag Rocks is an age-structured model (Earl

et al., 2023, Earl & Readdy, 2024, Casal2 Development Team, 2024) which estimates historical abundance and recruitment based on groundfish survey abundance and age composition, tag recapture rates, catch age compositions, catch per unit effort and biological data. The most informative data for the assessment comes from an extensive tag-recapture program implemented as part of the longline fishery. This approach assumes a closed population and that tagged fish are well mixed with non-tagged fish of the same age. Violations of these assumptions has the potential to produce biased estimates of stock abundance, status relative to targets and catch limits (Masere et al., 2024a, b). Current management is based on a 35-year projection (Constable, 2000) where estimates of historic recruitment are used to inform assumptions in the projection about the level and variability of future recruitment. However, in a variable or changing environment, these baselines may not reliably predict future population dynamics, and do not fully consider changing climate (Earl et al., 2024, Ouzoulias et al., 2024, Azmi et al., 2025). Moreover, although changes in distribution and biology are monitored, environmental parameters are not explicitly included in the assessment framework (Welsford et al., 2023). The CCAMLR Workshop on Climate Change (WS-CC-2023, SC-CAMLR-42, Annex 11) resulted in several recommendations directed to CCAMLR's Working Group on Fish Stock Assessment (WG-FSA) in this regard (Cavanagh and Pardo, 2024). WG-FSA has begun to address these, via its work plan, particularly in summarising evidence for changes in stock assessment and population parameters or processes that could be due to the effects of environmental variability or climate change (WG-FSA-IMAF-2024, paragraphs 7.9-7.14, Tables 19-23), including for Patagonian toothfish in Subarea 48.3 (WG-FSA-IMAF-2024, Table 19).

Here, we explore the relationship between Patagonian toothfish distribution and environmental factors that may govern their spatial distribution. By modelling species–environment relationships across multiple size-classes, we examine how toothfish habitat requirements and environmental constraints change throughout juvenile to adult life-stages. This work provides the basis for understanding the potential effects of climate change on the South Georgia Patagonian toothfish population to inform management of the fishery in a changing environment.

Methods

We divided our analyses into an investigation of distribution for early life-stages at South Georgia and Shag Rocks informed by demersal trawl data from scientific surveys, followed by a broader examination of adult spatial distribution across South Georgia and SSI informed by longline fishery data (**Figure 1**).

Data sources

Groundfish trawl survey data

To investigate the distribution of early life-stages at South Georgia we used information collected during groundfish surveys conducted approximately biennially on the South Georgia and Shag Rocks shelves between 1986 and 2023 (**Figure 1;** see ***Supplementary materials***, **Table S1**). Sampling methods have been consistent over time, consisting of 30-minute demersal trawls (120-foot otter trawl, 18-20 m wingspread, 3-6m headline height, 40 mm cod end mesh; Belchier et al., 2013) at a ship speed of ~3 knots carried out between nautical twilight at dawn and dusk. Surveys were predominantly carried out during the austral summer (November-February), except for 1997 and 2007 (August-September), 2008 (April), and 2021 (May; see **Table S1**). Trawl sampling encompassed the continental shelves of South Georgia and Shag Rocks at depths ranging from 75 to 700 m, although 95% of trawls were at depths less than 330 m. Nearshore and shallower areas (< 100 m), as well as locations directly south of South Georgia, were less frequently sampled due to accessibility and ground suitability (see Hollyman et al., 2021). For each trawl, total Patagonian toothfish abundance was recorded as well as trawl depth, trawl distance, and horizontal wingspread. In addition, the majority of captured toothfish caught were measured (total length; cm) allowing for catch totals to be separated by size-class.

To explore ontogenetic shifts in distribution, catch data were separated into six size-classes (**Table 1**) to obtain counts per haul for each size-class, with size-limits based on discrete modes represented in size-frequency data (**Figure S1**) and guided by known growth rates in juvenile Patagonian toothfish (~100-120 mm per year; Collins et al., 2010). While size-classes were established to reflect year-classes ranging from 1 to 6+ (or adult) Patagonian toothfish, at larger sizes (> 48 cm, putatively representative of age 4 fish) size-spectra often overlapped and were less distinct (**Figure S1**), such that size was a less

accurate proxy for age in the larger size-classes. As such, results from these analyses should be interpreted primarily with regards to size-dependent, rather than age-dependent, shifts in distribution. Throughout we refer to these size-classes via the shorthand notation $Sz_{lengths}$, where lengths indicates the length range (total length) in cm included in that size-class.

***Table 1**. Size-classes applied to Patagonian toothfish (Dissostichus eleginoides) caught in groundfish surveys at South Georgia and Shag Rocks. Ages are based on growth rates in Collins et al. (2010) and are indicative only. Larger size-classes may encompass individuals spanning two or more years of age.*

Size-class	Label	Size range (cm)	Age (years)
1	$Sz_{<26}$	≤ 25	1
2	$Sz_{26\text{-}37}$	26 - 37	2
3	$Sz_{38\text{-}47}$	38 - 47	3
4	$Sz_{48\text{-}57}$	48 - 57	4
5	$Sz_{58\text{-}66}$	58 - 66	5
6	$Sz_{>66}$	> 66	6+

Given the demersal trawl sampling approach, it is unlikely that all toothfish within the trawl area are captured (i.e., sampling efficiency < 1), such that catch-per-unit effort (CPUE) is an inherently biased estimate of local density. In particular, catches of the smallest size-class, < 26 cm, have been near-absent in particular years, despite the occurrence of a strong 26-37 cm size-class in the following year (Cavanagh et al., 2025). This discrepancy may arise due to gear selectivity, size-dependent net-avoidance behaviour, or more localized and patchy distribution of the smallest size-class. While these biases may vary among size-classes, there is no indication that they vary spatially. As such, results should be interpreted in terms of relative, rather than absolute, patterns in abundance.

Longline fishery catch data

Under CCAMLR Conservation Measures, fishing vessels are required to report details of their catch, including location, depth, number of hooks deployed, and any by-catch, on a haul-by-haul basis (CCAMLR C2). These data are available on request from the CCAMLR Secretariat, and for this study we requested catch and effort data (CCAMLR C2) from the toothfish fishery in CCAMLR Subareas 48.3 and 48.4 (CCAMLR Data Request 660). Requested data spanned the period from 1985 to 2023 and consisted of catch weight of Patagonian toothfish per haul, along with information on vessel, date,

depth (minimum and maximum), location, soak time, and number of hooks. Information on fishing operations in these regions, including changes to fishing regulations (depth limits, and seasons of operation) can be found in Abreu et al. (2024) and Belchier et al. (2022). Data were screened based on depth distribution and season, which resulted in the exclusion of data from years prior to 2005 and 2009 in Subareas 48.3 and 48.4, respectively, due to changes in fishing regulations and operation (seasonal opening and depth restrictions; **Figure S1 & S2**, ***Supplementary materials***). The resulting data covered the period where the minimum fishing depth was 700 m in both areas, and most lines were set at depths of 750-1750 m. Generally, fish captured by the fishery are greater than 60 cm (total length; Abreu et al., 2024) and estimates of selectivity suggest that 50% of fish are vulnerable to the fishery by age 8, reaching maximum vulnerability by age 10 (Earl et al., 2024). Given that, we use the term adult to refer to individuals captured in the fishery and use catch-per-unit effort (CPUE) according to catch weight per 1000 hooks as a coarse proxy for distribution of fish vulnerable to the fishery (i.e., within the horizontal and vertical operational range of the fishery), acknowledging that fishery-dependent data often provides a biased representation (Bishop, 2006). For the resulting dataset we also calculated day of year and lunar phase based on date, and average set depth and soak time (time elapsed between set start and haul start times in hours) to use as covariates in subsequent analyses.

Bathymetric and environmental data

Spatial data describing the variation in bathymetry and environmental variables were obtained for the South Georgia and Shag Rocks shelf (53-56°S, 33-44°W) region to identify the factors which may influence toothfish distribution as indicated by demersal trawl data. Bathymetry data were obtained from the ETOPO 2022 (2 km resolution) global relief model (NOAA 2022). Bathymetric data were also used to calculate seafloor slope and planform curvature using the terrain function in the raster package in R (Hijmans, 2025). Environmental variable datasets were obtained from the Copernicus Marine Service and consisted of daily maps (resolution ranging from 4 km to 0.083°) of surface (temperature, salinity, current speed, mixed layer thickness and log chlorophyll-a concentration) and seafloor (temperature, salinity; **Table 2**) conditions. In addition, we obtained temperatures at 93-110 m depth

in the water column, corresponding to vertical layer 22 of the 50 depth layers in the Global Physics Reanalysis dataset (GLORYS12V1, https://doi.org/10.48670/moi-00021; Lellouche et al., 2021), corresponding to conditions below the mixed layer that may be influential during early (egg, larvae, and initially after benthic settlement) developmental stages. For areas with seafloor depth shallower than 93 m (6% of shelf area less than 500 m depth), values from the closest available level were used, and only affected a small area as model predictions were restricted to depths sampled by trawls (70 to 1000 m). For all variables, we calculated the annual (January-December) climatological mean and variability (standard deviation across all constituent layers) calculated on a cell-by-cell basis across years from 1993 to 2023. However, apart from salinity, variability measures were excluded from subsequent analyses as they were highly correlated with the corresponding mean values ($|r| > 0.8$, **Table S2**).]] Values for each bathymetric and environmental variable were then assigned to trawls according to trawl mid-point location.

For analyses of longline CPUE for the South Georgia and SSI fisheries, we limited our analyses to an exploration of CPUE with respect to depth, recorded in-situ during fishery operations, and broad-scale patterns in seafloor temperature. The decision to focus on seafloor temperature was governed by the fact that adult toothfish are thought to be primarily benthic (Collins et al., 2010). Consequently, measures of distribution based on CPUE should be driven by seafloor, rather than surface, conditions. For each line we extracted seafloor temperature for the corresponding location from GLORYS12V1 (see **Table 2**). Values for seafloor temperature were extracted on the day the line was set (dynamic) as well as the climatological average seafloor temperature (static; averaged over 2005-2023, to match the fishing time-period), and we test models containing one of the two variables to see which measure provides the better fit to the data.

Table 2. *Trawl and environmental covariates, data sources, and processing information for variables included in Patagonian toothfish (Dissostichus eleginoides) distribution analyses. All variables listed were used primarily in construction of distribution models for the South Georgia and Shag Rocks shelf based on demersal trawl survey data. However, seafloor temperature data from the Global Ocean Physics Reanalysis dataset (GLORYS12V1) were also used in analyses of broad-scale distribution from the longline fishery data. Covariates listed represent the climatological mean and variability calculated across all daily layers for the specified time-range.*

Variable	Description	Source	Time-range	Resolution
survey	Survey categorical variable			survey
date	Survey mid-point date			survey
sun	Sun altitude above the horizon (radians)			trawl
area	Area swept during trawl in km^2			trawl
depth[a]	Seafloor depth			
slope	Seafloor slope, calculated from depth	ETOPO 2022		2 km
curve	Seafloor planform curvature, calculated from depth			
SST	Mean sea surface temperature (SST)	Global Ocean OSTIA SST[b]	1993-2023	0.0167° daily
SFT	Mean temperature at the seafloor (SFT)			
MWT	Mean mid water column temperature at 100 m			
SSAL	Mean sea surface salinity			
SSAL_sd	Variability (SD) of sea surface salinity	Global Ocean Physics Reanalysis[c]	1993-2023	0.083° daily
FSAL	Mean salinity near the seafloor			
FSAL_sd	Variability (SD) of salinity near the seafloor			
VEL	Mean surface current speed			
MLT	Mean mixed layer thickness			
CHL	Mean surface chlorophyll-a concentration	Global Ocean Colour[d]	1997-2023	4 km daily

a: In-situ trawl depth was used in model fitting, with ETOPO 2022 bathymetry data used for prediction
b: Copernicus Data Store: sst_glo_sst_l4_rep_observations_010_011, https://doi.org/10.48670/moi-00165
c: Copernicus Data Store: global_multiyear_phy_001_030, https://doi.org/10.48670/moi-00021
d: Copernicus Data Store: oceancolour_glo_bgc_l4_my_009_104, https://doi.org/10.48670/moi-00281

Distribution models - South Georgia and Shag Rocks shelf

Model framework

For each size-class of Patagonian toothfish captured during groundfish surveys at South Georgia and Shag Rocks (**Table 1**), we fitted models to identify and explore the variables and relationships that best describe patterns in spatial distribution. Distribution models were constructed using Generalized Additive Models (GAMs) to accommodate non-linear functions of environmental/bathymetric covariates (henceforth referred to as habitat covariates) and were fitted to size-class specific counts (response: count per trawl) from each trawl across the 28 groundfish surveys available (**Table S1**). All

models were fitted using the gam function in the mgcv package in R fitted via restricted maximum likelihood (REML; Wood 2011) assuming counts were distributed according to a negative binomial distribution (nb family, log-link). Prior to model fitting, habitat covariates were transformed where necessary to reduce the potential for outliers, then scaled and centred to aid model fitting.

Several components were included in all models to account for differences among trawls unrelated to spatial variability in abundance. Smooths for date and survey random effects were included to account for long-term trends and interannual variability among surveys, respectively, and time of day was included via a smooth based on sun altitude to model potential diel vertical movement. An offset term of log-transformed trawl area (horizontal wingspread × trawl distance; km^2) was also included to account for variable trawl effort.

Models were then constructed by adding smooths for habitat covariates (**Table 2**) using a forward stepwise approach based on maximising predictive accuracy. This stepwise approach was repeated up to a maximum of five possible habitat covariates, exploring all possible additions at each stage, such that models conformed to:

$$\log(\hat{y}_i) = \log(A_i) + \mu_0 + \alpha_{S_i} + s(t_{S_i}) + \sum_{j=1}^{j\leq 5} s_j(x_{j,i})$$

$$y_i \sim NB(\hat{y}_i, \hat{\theta})$$

[eqn. 1 & 2]

where $\hat{y}_i$ is the fitted value for trawl *i*, with count y_i, $\log(A_i)$ is an offset term of area swept, μ_0 is the intercept, α_{S_i} is a survey random effect, $s()$ are smooth functions of survey mid-date, t_{S_i}, and habitat covariates x_j, and $\widehat{\theta}$ is the negative binomial dispersion parameter. At each step, model statistics were checked, and further model development was only permitted for a given combination of covariates if it resulted in higher predictive accuracy relative to the previous step (i.e., minus the latest addition) and had a maximum concurvity (the ability of a smooth for one covariate to be approximated by other

terms; Wood 2008) across covariates of less than 0.7. Predictive accuracy was calculated via 10-fold cross-validation using a log-likelihood score statistic equal to the summed log-likelihood of the held-out observations (one of the ten folds) given model predicted values for that cross-validation fold (Dormann et al.,2018):

$$\mathcal{L}_m = \sum_{j=1}^{j=10} \ell\left(\boldsymbol{y_j} | \, \hat{\boldsymbol{y}}^{\boldsymbol{m}}_{\boldsymbol{y}_{[-j]}}, \hat{\theta}^{m}_{y_{[-j]}}\right)$$

[eqn. 3]

where $\mathcal{L}_m$ is the likelihood score across folds, *j*, for a specific model, *m*, and $\ell\left(\boldsymbol{y_j} | \, \hat{\boldsymbol{y}}^{\boldsymbol{m}}_{\boldsymbol{y}_{[-j]}}, \hat{\theta}^{m}_{y_{[-j]}}\right)$ is the log-likelihood of observations $\boldsymbol{y_j}$ in the held-out data given predicted values $\hat{\boldsymbol{y}}^{\boldsymbol{m}}_{\boldsymbol{y}_{[-j]}}$ and negative binomial dispersion parameter, $\hat{\theta}^{m}_{y_{[-j]}}$, from the model fitted to data excluding fold *j* (indicated by $\boldsymbol{y}_{[-\boldsymbol{j}]}$). The resulting statistic was converted to a measure *D* that varies from 0 to 1, with 0 indicating the model predicts no better than a null model with no spatial components (only survey and area offset terms), and 1 indicating perfect prediction (see ***Supplementary materials*** for more information on cross-validation approach). For each size class, results are presented for the model with highest predictive accuracy, and for models containing only temperature and depth covariates to examine the predictive capacity of alternate temperature metrics.

Habitat relationships and density maps

Habitat relationships were visualised through partial dependence plots. These were created by first calculating the expected CPUE predicted by the model across the range of values exhibited by a particular habitat covariate, holding all other terms constant. Given differences in absolute abundance among size-classes, the predicted values, $\hat{y}_i$, were converted to relative density, $\hat{z}_i$, by dividing by the mean across predicted values.

$$\hat{z}_i = \frac{\hat{y}_i}{\frac{1}{n}\sum_{j=1}^{n} \hat{y}_j}$$

[eqn. 4]

where *n* signifies the number of predicted values. Plots of relative (rather than absolute) density are therefore easier to compare given differences in CPUE among size-classes. Rather than present results for the singular best model (although see ***Supplementary materials*** for model-specific plots), which may omit certain habitat covariates, we instead average predicted relative density $\hat{\boldsymbol{z}}$ across all fitted models, weighted according to each model's log-likelihood score:

$$\bar{\boldsymbol{z}} = \sum_{i \in M} w_m \, \widehat{\boldsymbol{z}_{\boldsymbol{m}}}$$

$$w_m = \frac{e^{-\mathcal{L}_m}}{\sum_{i \in M} e^{-\mathcal{L}_i}}$$

[eqn. 5 & 6]

where $\bar{\boldsymbol{z}}$ is the model-averaged set of relative density estimates, across model-specific estimates, $\widehat{z_m}$ and model weights, w_m, and where the sum in the denominator for w_m is evaluated over the model set, M. The resulting weights favour relationships estimated by models with higher predictive accuracy as measured via cross-validated log-likelihood (Dormann et al., 2018).

Maps of toothfish density (individuals km^{-2}) were created by using models to predict values onto a 2×2 km resolution grid populated with habitat covariates projected from their native grid. A 2 km grid was chosen to match the bathymetry data, which had the highest resolution, to best visualise distribution patterns according to bathymetric features (i.e., canyons) on the South Georgia shelf. When making predictions, date was set to January-2023 so that predictions represent present day values, sun angle was set to 0.5, equal to the median value in the dataset, and area-swept was set to 1 km^2 such that predicted values represented abundance per km^2. As with habitat relationships, we adopt an ensemble approach to model prediction, whereby predicted maps were created for each model and then averaged, weighted by the predictive likelihood score of the corresponding model. Maps representing individual model uncertainty (CV = standard error divided by mean of predicted densities) were also

created using the best-predicting model as a reference and are presented in the ***Supplementary materials***.

Broad scale analyses of adult Patagonian toothfish distribution in the Scotia Sea

Longline data analyses

Separate analyses, although founded on the same approach, were performed on catch data (response: catch weight per haul) from the South Georgia and SSI longline fishery. For each area, models were fitted to catch weight using GAMs with random effects to control for variation among vessels and years and an offset term (log(hook count)) to control for differential effort among sets. To the base model containing offset and random effects terms, we then added smooth terms (thin-plate regression splines) for date, set depth, day of year, lunar phase, soak time, and bottom temperature to explore potential effects of each. Spatial fields, modelled via Gaussian process smoothers according to easting and northing coordinates, were also included to account for spatial autocorrelation. Models were fitted assuming a tweedie distribution (family = tw) for catch weights, such that:

$$\log(\widehat{y_i}) = \log(H_i) + \mu_0 + \alpha_{1,V_i} + s(E_i, N_i) + s(Y_i) + s(D_i) + s(J_i) + s(L_i) + s(S_i) + s(BT_i)$$

$$y_i \sim TW(\widehat{y_i}, \hat{\sigma}^2, \hat{\rho})$$

[eqn. 7 & 8]

where $\widehat{y_i}$ is the expected catch for line *i* given observed catch y_i, H_i is the number of hooks, μ_0 is the intercept, α_{1,V_i} are random year by vessel effects, $s(.)$ are smooth terms for easting, E_i, and northing, N_i (gaussian process), year, Y_i, depth, D_i, day of year, J_i, lunar phase, L_i, soak time, S_i, and bottom temperature, BT_i, and $\hat{\sigma}^2$ and $\hat{\rho}$ are the estimated variance and power parameters for the tweedie distribution. To simplify model fitting and evaluation, all smooth terms were specified as the shrinkage variant of the thin-plate regression spline smoother (basis = 'ts'), which results in uninformative model components being removed automatically as part of the smoothing parameter selection process (Marra and Wood, 2011). As seafloor temperature covaries with depth and location, we fitted alternate models, varying the inclusion of depth, seafloor temperature, and spatial field to investigate whether

the inclusion of depth or location confounding factors altered fitted temperature relationships. Furthermore, each model variant was fitted using either dynamic, or climatological mean temperature covariates to identify the best-fitting temperature covariate. Alternate models were ranked based on Akaike's Information Criterion (AIC), and we present results for the model with lowest AIC.

Additional factors that have previously been shown to influence catch rates (soak time, gear type, cetacean presence or abundance during hauling - indicating depredation; Earl et al., 2021) were not included in this analysis due to the focus on key environmental factors.

Spatial variation in CPUE and seafloor temperatures for the longline fishery areas

In addition to the analyses outlined above, we also explored spatial variation in longline catch data to identify the correspondence with water temperatures around South Georgia and Shag Rocks, and towards their southern range edge at the South Sandwich Islands. For each area, spatial variation in Patagonian toothfish CPUE (catch weight per 1000 hooks) was visualised by calculating the mean CPUE of all lines set within 10×10 km grid cells covering the extent of the longline fishery, which extends to the southern part of the SSI chain where Antarctic toothfish dominate the catch (*Dissostichus mawsoni*; Soeffker et al., 2022). This was then compared to climatological average temperatures at the seafloor in each region, and also by visualising temperatures across the longitudinal or latitudinal span of the South Georgia and SSI regions, respectively, at depths of 1063-1246 m and 1246-1453 m, capturing the depth range at which the fishery operates. For SSI, we also evaluated temperatures throughout the entire water column using a cross-section along a latitudinal transect along the SSI chain. Temperature data used in these analyses were obtained from the GLORYS12V1 dataset (https://doi.org/10.48670/moi-00021), with climatological average temperatures at the seafloor and for each depth-level (cross-section approach) calculated over data from 2005 to 2023.

Temperature trends in the Scotia Sea

To provide a large-scale overview of variation and trends in temperature throughout the known range of Patagonian toothfish in the Scotia Sea, we analysed year-average sea surface temperature (SST) and water column temperatures at a range of depths for Shag Rocks, South Georgia, and the SSI chain. We

divided the SSI chain into three sections to represent areas where Patagonian toothfish are frequently (northern: north of 57°S) versus rarely (southern: 58.2-60.5°S) caught by the longline fishery, with the central section (57-58.1°S) representing the transitional zone. Temperature data were obtained from the Global Ocean OSTIA (SST) and Global Ocean Physics Reanalysis datasets (water column temperature) for the 30-year period covering 1994 to 2023. Extracted data were cropped to the 2000 m isobath for each area (Shag Rocks = 40-44°W, South Georgia = east of 40°W), and then averaged over space and time to produce annual measures of temperature for each area for the following strata: 60-101 m (GLORYS12V1 vertical levels 20-22), 101-204 m (levels 23-26), 204-417 m (levels 27-30), 417-833 m (levels 31-34), 833-1349 m (levels 35-37), and 1349-1813 m (levels 38-39). These strata were chosen to represent putative depth ranges inhabited by Patagonian toothfish from larvae and small juvenile fish (surface, 60-101 m and 101-204 m), through intermediate sized juveniles (204-417 m), and finally adults (depth 500-2000 m). Trends in temperature were estimated for each area and depth strata by fitting a linear model with year as the independent variable using Generalised Least Squares (GLS, package nlme; Pinheiro and Bates, 2025) with a first-order autoregressive correlation structure (AR1) to account for temporal autocorrelation between years. Trend estimates, and their uncertainty (95% confidence interval), were used to identify the areas and depth strata with the largest changes over the 1994-2023 period.

Unless otherwise specified, all analyses and data processing were performed in R version 4.3.3 (R Core Team 2024).

Results

Distribution models - South Georgia and Shag Rocks shelf

Spatial patterns of Patagonian toothfish abundance consistently showed relationships with depth and temperature across all size-classes (**Table 3**). In almost all instances, models containing depth and one of the three temperature covariates (mean sea surface temperature, SST; midwater temperature at 100 m depth, MWT; seafloor temperature, SFT) represented considerable improvements in predictive accuracy compared to models only including depth (**Table 3**). Across all size-classes investigated,

models containing SST or midwater temperature outperformed those containing seafloor temperature based on predictive accuracy (**Table 3**). Furthermore, for all size-classes barring 38-47 cm and > 66 cm categories, the best performing model containing just temperature and depth had comparable predictive accuracy (pD within 0.01) to the best performing models that contained additional habitat covariates (**Table 3**). Predictive accuracy scores calculated via cross-validation ranged from 0.148 (58-66 cm) to 0.313 (< 26 cm), suggesting that model predictions were accounting for ~15-30% of the spatial variation among trawls in our dataset (**Table 3**).

Depending on size-class, models with highest predictive accuracy either included temperatures at the surface (< 26 cm to 48-57 cm size-classes) or at 100 m depth (58-66 cm, > 66 cm size-classes and total abundance); however, SST and MWT were largely interchangeable and produced similar models and predictions due to the high correlation between them. Covariates associated with seabed morphology (slope and planform curvature) were frequently included in the set of best models, being absent only for the < 26 cm size-class, as were covariates associated with mixed layer thickness (MLT), chlorophyll-a concentration, seafloor temperature and salinity (**Table 3**). However, which variables were included in the best predicting models was size-class dependent, changing from inclusions of planform curvature, MLT and chlorophyll-a concentration for < 26 cm to 38-47 cm size-classes, to models including seabed slope, and variation in salinity for 48-57 cm to > 66 cm size-classes (**Table 3**). Notably, seafloor temperature was included in the best-predicting model for intermediate size-classes (38-47 cm and 48-57 cm) but was absent from models for smaller and larger size-classes (**Table 3**).

Table 3. *Statistics for distribution models fitted to Patagonian toothfish (Dissostichus eleginoides) counts from South Georgia and Shag Rocks groundfish surveys. Models containing depth and a single temperature covariate are presented alongside the four best models based on predictive accuracy. Statistics are the estimated degrees of freedom (edf), the difference in AIC (ΔAIC) relative to the model with highest predictive accuracy, and prediction accuracy score (pD) from cross-validation, which varies from 0 (no improvement over the null) to 1 (predicted values perfectly). All covariates are annual climatological mean values, unless otherwise specified, and include: sea surface temperature (SST), seafloor temperature (SFT), midwater temperature at 100 m depth (MWT), mixed layer thickness (MLT), surface salinity mean (SSAL) and variability (SSAL_sd), chlorophyll-a concentration (CHL), seabed planform curvature (curve) and slope, surface current speed (VEL), and variability in seafloor salinity (FSAL_sd).*

	Depth + temperature models				**Best predicting models**			
Size (cm)	**Model[a]**	**edf**	**ΔAIC**	**pD**	**Model[a]**	**edf**	**ΔAIC**	**pD**
< 26	Depth	24.5	151	0.200	**+ MWT + MLT + SSAL**	**30.7**	**0.0**	**0.313**
< 26	+ SST	25.9	17.9	0.276	+ MWT	23.0	14.0	0.313
< 26	**+ MWT**	**23.0**	**14.0**	**0.313**	+ MWT + SSAL	26.4	10.4	0.310
< 26	+ SFT	25.8	90.2	0.255	+ MWT + SFT	25.7	12.7	0.309
26-37	Depth	27.5	388	0.014	**+ MWT + CHL + curve + MLT**	**42.9**	**0.0**	**0.215**
26-37	+ SST	37.0	23.5	0.203	+ MWT + SFT + CHL + MLT	45.6	-20.3	0.213
26-37	+ MWT	37.9	23.1	0.200	+ MWT + CHL + slope + MLT	42.7	6.0	0.212
26-37	+ SFT	33.2	228	0.108	+ MWT + CHL + MLT	41.7	4.2	0.211
38-47	Depth	34.2	511	-0.030	**+ MWT + SFT + CHL + curve**	**51.3**	**0.0**	**0.179**
38-47	+ SST	38.2	69.2	0.148	+ MWT + SFT + CHL	50.3	0.4	0.178
38-47	+ MWT	39.4	59.4	0.153	+ MWT + SFT + CHL + VEL	52.9	-4.5	0.178
38-47	+ SFT	39.8	245	0.097	+ MWT + SFT + CHL + slope	53.1	-4.0	0.177
48-57	Depth	34.2	353	0.004	**+ MWT + SFT + slope + SSAL_sd**	**50.1**	**0.0**	**0.186**
48-57	+ SST	37.1	36.3	0.137	+ MWT + slope + SSAL_sd	42.8	6.0	0.186
48-57	+ MWT	36.6	21.4	0.180	+ MWT + SFT + SSAL_sd	47.3	3.8	0.186
48-57	+ SFT	39.0	161	0.112	+ MWT + slope	37.2	8.3	0.184
58-66	Depth	29.2	103	0.096	**+ SST + slope**	**38.0**	**0.0**	**0.148**
58-66	+ SST	35.1	0.4	0.142	+ SST + slope + MLT	38.8	-0.9	0.146
58-66	+ MWT	34.8	3.6	0.139	+ SST + slope + FSAL_sd	39.1	1.4	0.145
58-66	+ SFT	32.3	55	0.123	+ SST + slope + SSAL_sd	39.2	-4.3	0.145
> 66	Depth	27.1	39.2	0.120	**+ SST + FSAL_sd**	**29.2**	**0.0**	**0.240**
> 66	+ SST	29.8	17.8	0.191	+ SST + FSAL_sd + curve	32.8	-2.9	0.232
> 66	+ MWT	31.0	14.9	0.174	+ SST + FSAL_sd + SSAL_sd	31.8	4.5	0.230
> 66	+ SFT	33.4	34.0	0.052	+ SST + FSAL_sd + MLT	30.3	1.9	0.227
All	Depth	34.4	821	-0.010	**+ SST + SFT + FSAL_sd + curve**	**52.9**	**0.0**	**0.195**
All	+ SST	38.9	45.5	0.188	+ SST + SFT + FSAL_sd	46.8	-2.0	0.193
All	+ MWT	38.9	59.5	0.164	+ SST + CHL + curve	49.3	1.4	0.193
All	+ SFT	39.6	412	0.091	+ SST + SFT + curve	51.3	3.4	0.192

a: Depth is omitted in model descriptions to save on space but was included as a covariate in all models presented here

Fitted relationships for depth were indicative of a shift towards deeper water with increasing size, shifting from depths of less than 200 m (peak density at 110 m) for < 26 cm fish, to depths of 200-400

m (peak density at 300 m) in 26-37 cm, and 38-47 cm fish, followed by a transition to waters deeper than 400 m for the largest size-classes (**Figure 2**). Except for the smallest and largest size-classes that displayed monotonically decreasing/increasing relationships with depth, respectively, remaining size-classes displayed either a major (26-37 cm, 38-47 cm) or minor (48-57 cm, 58-66 cm) peak in abundance at ~ 300 m, suggesting that 300 m represents an optimum intermediate depth as toothfish grow at South Georgia (**Figure 2**). The bimodal relationship estimated for 26-37 cm fish also suggests that this size-class represents the first transitional stage from the very shallow preferences exhibited by smaller (< 26 cm) fish to the deeper habits exhibited by larger (38-47 cm) fish (**Figure 2**).

For all size classes, predicted abundances increased with surface and/or midwater temperatures, with major break points at SST = 1.8°C and MWT = 1.2°C (**Figure 2**). For the two largest size classes, while higher abundances were predicted in locations with warmer near surface conditions, there was less variability in predicted abundance according to SST or MWT, suggesting that the coupling between distribution and near-surface temperatures relaxes as fish grow (**Figure 2**).

In contrast to temperature and depth, which have relatively larger effects on predicted distribution, the remaining habitat covariates displayed weaker effects (**Figure 2**). Seabed planform curvature (26-37 cm and 38-47 cm) and slope (48-57 cm and 58-66 cm) effects were suggestive of higher abundance in canyons (negative planform curvature) for smaller fish, as well as overall abundance, followed by a transition to shelf edge habitats (higher slope) at, or prior to, 48-57 cm (**Figure 2**). Seafloor temperature was included in models for 38-47 cm, 48-57 cm and overall fish abundance, suggestive of a preference for locations which average 1.5-2.1°C, with a peak at year-averaged seafloor temperatures of 2°C (**Figure 2**). Abundance overall, and for fish > 66 cm, also varied with annual variability in seafloor salinity, suggestive of higher abundance in locations that have more variable salinity (**Figure 2**). Fitted relationships for chlorophyll-a concentration and mixed-layer thickness were complex and displayed a high degree of uncertainty, indicative of weak and/or location-specific effects that are not easily characterized (see **Figures S4-S10** for model outputs from the highest ranked model for each size class).

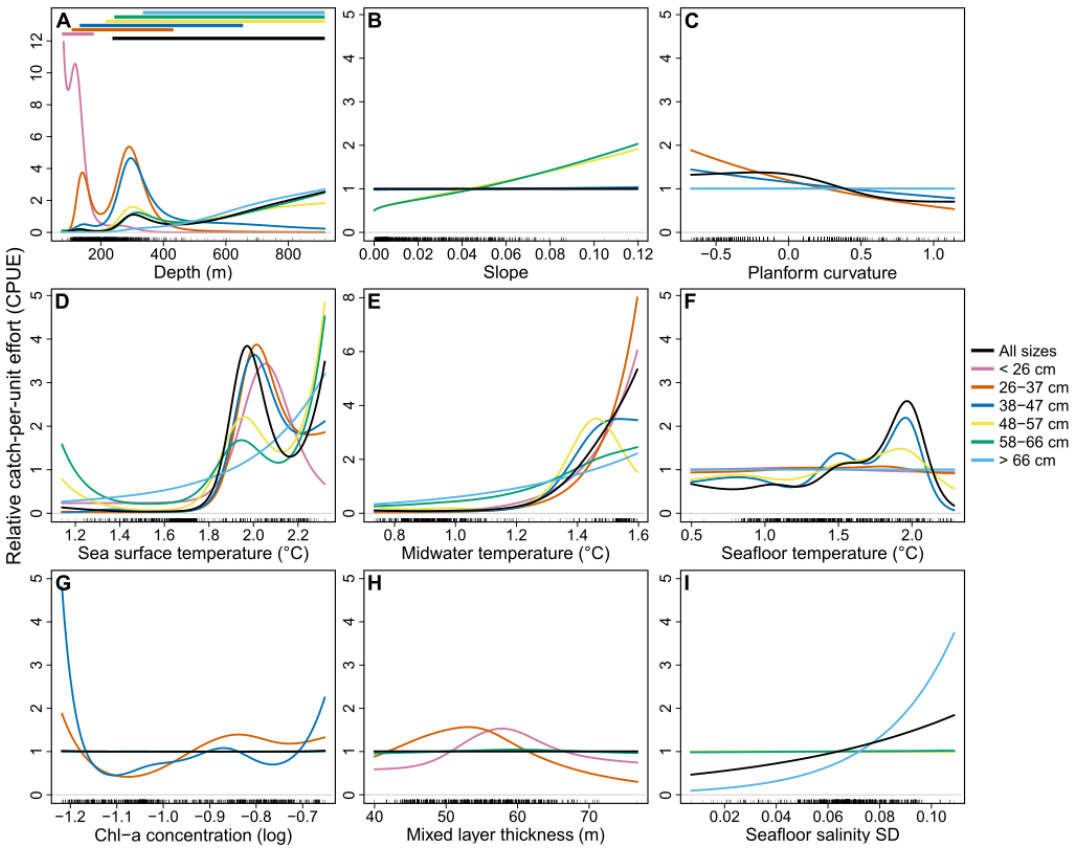

Figure 2. *Model-averaged habitat covariate relationships estimated in distribution models for Patagonian toothfish (Dissostichus eleginoides) at South Georgia and Shag Rocks fitted based on demersal trawl data. Relationships are shown for covariates included in the best model for at least two size-classes and include seafloor depth (**A**), slope (**B**) and planform curvature (**C**), mean temperatures at the surface (SST; **D**), 100 m depth in the water column (**E**) and seafloor (**F**), and log-transformed chlorophyll-a concentration (**G**), mixed layer thickness (**H**) and variation in seafloor salinity (**I**). Values on the y-axis are relative CPUE, equal to model predicted values divided by the mean of those predictions across the covariate range, holding all other covariates constant, such that plotted values are comparable across size-classes. Horizontal bars in the upper portion of (**A**) show the depth range over which the estimated function exceeded 10% of the maximum, to indicate ontogenetic changes in depth. Apart from depth (**A**) and midwater temperature (**E**), y-axis scales are identical to highlight differences in effect magnitude among covariates.*

Size-specific distributions – South Georgia and Shag Rocks

Predicted distributions resulting from these models indicate a largely restricted distribution on the Shag Rocks shelf for the < 26 cm size-class, which expands to encompass much of the Shag Rocks shelf for the 26-37 cm size-class (**Figure 3**). While much of the predicted abundance for these two size-classes were restricted to the Shag Rocks shelf (85% and 90% for < 26 cm and 26-37 cm fish, respectively), models also predicted lower densities in the nearshore environment and in the canyons around South Georgia for < 26 cm and 26-37 cm fish, respectively, which was also evident from survey

trawls (**Figure 3**). However, nearshore areas around South Georgia have much lower, often zero, survey coverage leading to higher uncertainty, so we note caution when interpreting these results (refer to **Figure S11** for maps showing prediction uncertainty). Predicted distributions of 38-47 cm and 48-57 cm fish are indicative of a transition away from the Shag Rocks shelf, progressing toward the Shag Rocks shelf break, along with higher densities around the South Georgia shelf edge (27% of predicted 48-57 cm fish abundance around South Georgia, compared to 10% for 26-37 cm fish) and in canyons extending onto the shelf (**Figure 3**). Our models also indicate that areas on Shag Rocks shallower than 300 m are devoid of the largest size-class of toothfish we investigated, and that comparable densities occur off-shelf around South Georgia (44% of predicted > 66 cm fish abundance) to those around Shag Rocks (**Figure 3**). However, predicted peak densities remained highest at the northwest end of Shag Rocks, in addition to the eastern South Georgia shelf edge that was predicted to have high densities of 58-66 cm fish (**Figure 3**). Patterns of abundance, irrespective of size, show a bias towards Shag Rocks with 87% of the total abundance (depths 70-1000 m) predicted there compared to around South Georgia, with major hotspots on the South Georgia shelf confined to canyons and the shelf edge (**Figure 3**). However, for the two largest size-classes we note caution when interpreting these results as the depth range covered during groundfish surveys only consistently samples a small portion at the upper limit of the known depth range of adult toothfish.

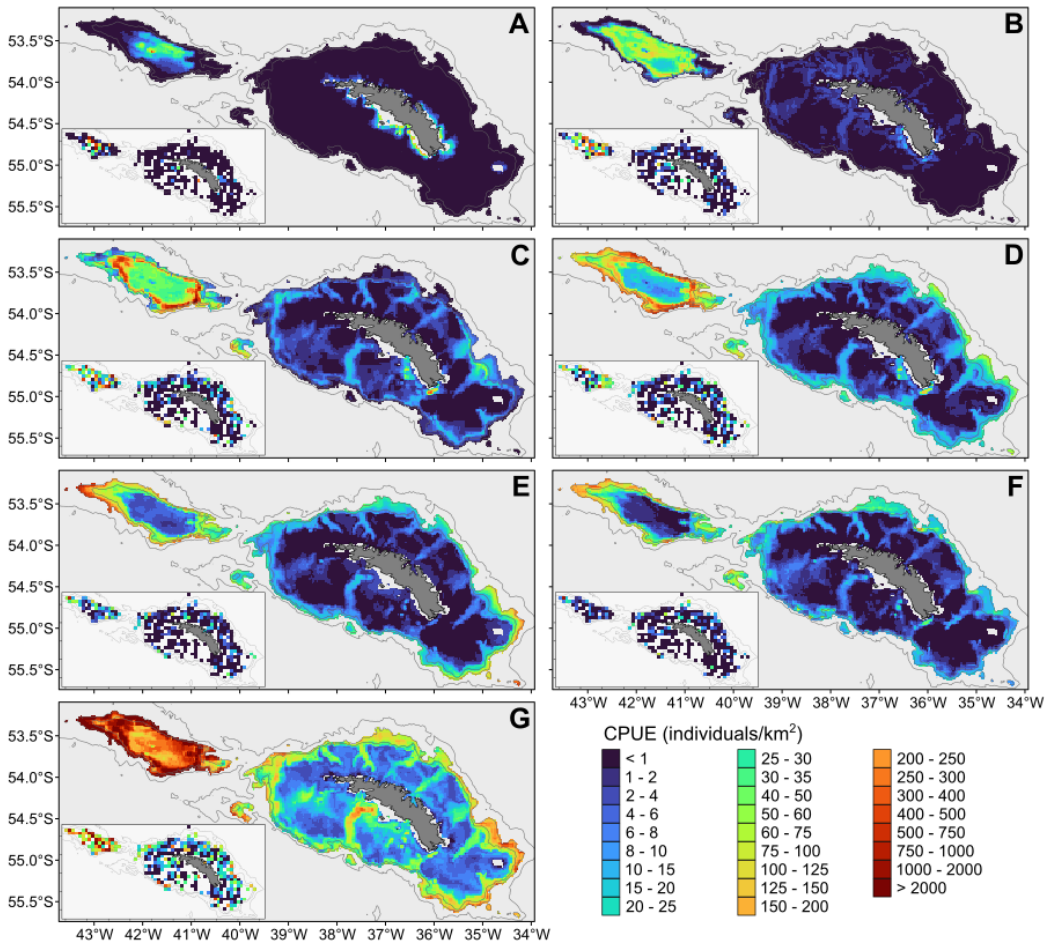

Figure 3. *Model predicted densities of Patagonian toothfish (Dissostichus eleginoides) for size-classes of < 26 cm (**A**), 26-37 cm (**B**), 38-47 cm (**C**), 48-57 cm (**D**), 58-66 cm (**E**), > 66 cm (**F**), and for all sizes (**G**) around South Georgia and Shag Rocks. Predicted distributions are shown according to fitted bathymetric and environmental relationships, with temporal covariates kept constant (date = 2023, sun angle = 0.5), and limited to seafloor depths of 70-1000 m, matching the depth range sampled during groundfish surveys. Inset maps in each panel show the spatial distribution of observed mean catch-per-unit-effort (10 km grid resolution) across all trawls for the corresponding size-class. The 500, 1000 and 2000 m isobaths are plotted (grey lines).*

Estimated Patagonian toothfish distribution from longline data

Analyses based on CPUE of Patagonian toothfish from the South Georgia and South Sandwich Island longline fisheries were indicative of a positive relationship between CPUE and seafloor temperatures (SFT) in both regions. Models containing climatological mean SFT had lower AIC compared to those containing dynamic SFT (**Table S3**), although models containing dynamic SFT also indicated a positive relationship between SFT and CPUE.

While positive, the fitted relationship between CPUE and SFT around South Georgia and Shag Rocks was small, with relative CPUE remaining near constant throughout much of the temperature range (0.7-2.3°C) and only varying from the mean for temperatures above 2°C (**Figure 4**). This matches the observed pattern of average CPUE, which shows no consistent change along the major west to east gradient in SFT in this region (**Figure 4**). Spatial analyses did indicate the occurrence of CPUE hotspots, but these were sporadically located and were seemingly unrelated to SFT (**Figure S12**). Analyses were also indicative of seasonal variation in CPUE around South Georgia, with CPUE decreasing prior to/during the spawning season (June-August), as well as a decline in CPUE at depths greater than 1700 m (**Figure S12**). We acknowledge that CPUE in this region may better reflect catch efficiency rather than local density and that this needs to be considered when interpreting these results.

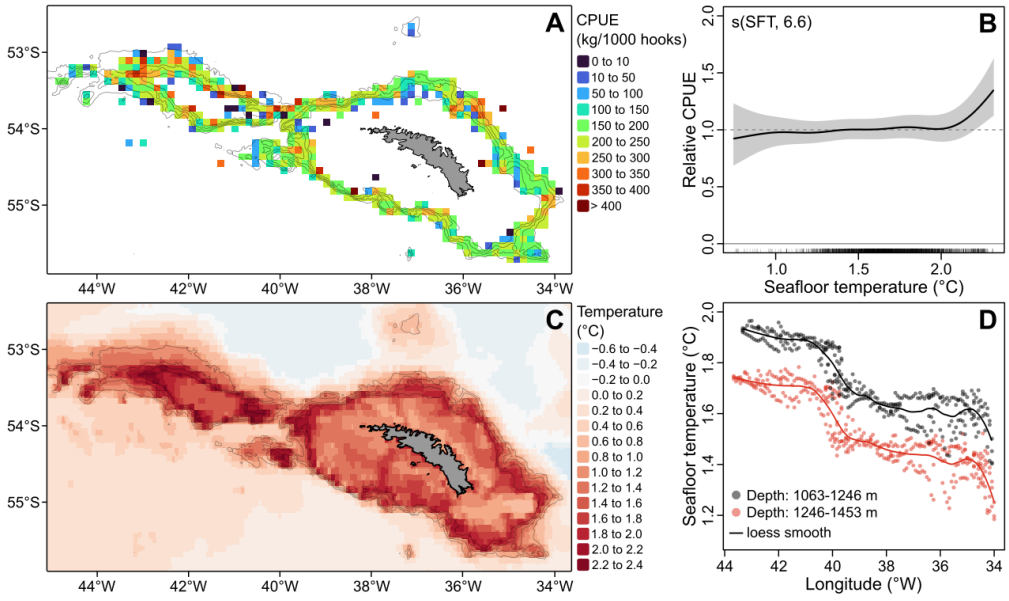

Figure 4. *Distribution of adult Patagonian toothfish (Dissostichus eleginoides) catch-per-unit effort (CPUE) from longline catch data in relation to seafloor temperature at South Georgia. The mean CPUE (**A**) across all lines set between 2005 and 2023 per 10 km grid cell is shown as a proxy for broad-scale distribution. The relationship between CPUE and seafloor temperature (**B**) for the South Georgia longline fishery from a Generalised Additive Model is shown as the mean and 95% confidence interval (shading) of the estimated relationship scaled to relative CPUE by dividing by the mean fitted value across the functions range. Spatial variation in seafloor temperatures is plotted as a map (**C**) and according to longitude (**D**) for seafloor depths of 1063-1246 m and 1246-1453 m around the South Georgia and Shag Rocks shelf edge, corresponding to the main depths targeted by the fishery. Values plotted in (**C**) and (**D**) represent climatological annual mean temperatures from 2005 to 2023 extracted from the Global Ocean Physics Reanalysis dataset (Table 2).*

At the South Sandwich Islands, the estimated relationship between CPUE and SFT was indicative of a step-like transition between 0.2 and 0.3°C potentially suggesting a lower thermal limit for Patagonian toothfish in this region (**Figure 5**). Examination of seafloor temperatures along the SSI chain indicate that this temperature threshold coincides with the decrease in temperature south of Saunders Island, which demarcates the division between areas where Patagonian toothfish are frequently caught (north) from those where they are seemingly absent (south) (**Figure 5**). Inclusion of spatial variation into our models did improve model fit but acted to obscure this temperature relationship as it accounted for the same latitudinal variation in CPUE, while also identifying CPUE hotspots in the northern part of the SSI chain (**Figure S14**). Despite that, a step-like temperature effect was still evident in that model, reaching an asymptote at 0.2°C (**Figure S14**). However, we opt to show the result for the model without the spatial field (i.e., **Figure 5B**) as we believe it more accurately captures the effect of this temperature gradient on toothfish CPUE. Latitudinal gradients in temperature at depths where the fishery operates (1063-1453 m) indicate that temperatures vary little with latitude across the northern (0.3 - 0.5°C) and southern (0.1 - 0.3°C) portions of the SSI chain but decrease by 0.2°C between the two areas (**Figure 5**). While temperatures north of Saunders Island are warmer, and therefore more favourable for Patagonian toothfish, the lower occurrence of Patagonian toothfish further south may also be linked to the two deep-water passages north and south of Saunders Island (**Figure 5**). In both passages, average temperatures near the seafloor are less than 0.0°C, which may act to inhibit transit between the two areas (**Figure 5**). In addition to temperature and spatial variation, our analyses of longline catch data also indicated that CPUE appeared to increase between 2009 and 2013, followed by a declining trend from 2013 onwards (**Figure S13**).

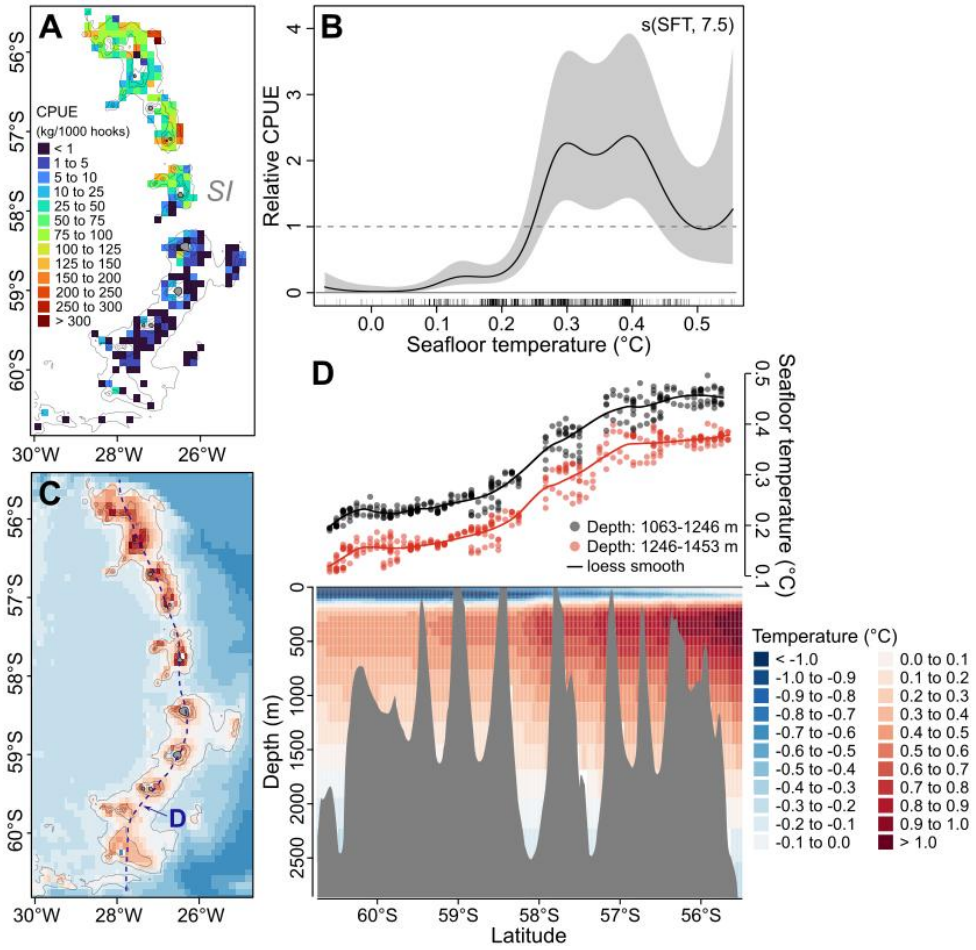

Figure 5. *Patagonian toothfish (Dissostichus eleginoides) distribution in relation to temperature along the South Sandwich Island (SSI) chain. Spatial distribution of Patagonian toothfish (**A**) is shown via the mean catch-per-unit effort (CPUE) across all lines set between 2009 and 2023 per 10k m grid cell. The location of Saunders Island (SI), referred to in the main text, is also shown. The relationship between CPUE and seafloor temperature (**B**) for the SSI longline fishery from a Generalised Additive Model is shown as the mean and 95% confidence interval (shading) of the estimated relationship scaled to relative CPUE by dividing by the mean fitted value across the functions range. Temperatures at the seafloor (**C**) and throughout the water column (**D**) along a transect spanning the SSI chain (dashed line in **C**) are also shown and represent climatological annual mean temperatures from 2009 to 2023 extracted from the Global Ocean Physics Reanalysis dataset.*

Temperature trends across the Patagonian toothfish range in the Scotia Sea

Over the last 30 years (1994-2023) sea surface temperatures (SST) increased in each area examined, with trend estimates varying from 0.07°C/decade (95% CI: -0.03 to 0.18) in the southern part of the SSI chain to 0.17°C/decade (95% CI: 0.05 to 0.28) at South Georgia (**Figure 6**). While warming trends were evident for most sub-surface depth strata, temperatures appeared to have remained stable or cooled over the same time-period at depths of 223-454 m and 110-223 m, respectively (**Figure 6**).

Further examination of temperature at those depth strata indicated relatively higher interannual variability, along with a non-linear trend through time with temperatures decreasing from 2005-2007 relative to pre-2005 levels, followed by static (SSI) or increasing trends (South Georgia, Shag Rocks) from then onwards (**Figure S15**). Whilst temperatures at these depths may not be relevant to Patagonian toothfish in the SSI, given the presumption of a largely adult population, the relatively higher interannual variability is suggestive of less predictable conditions for juvenile toothfish at South Georgia. At depths greater than 454 m, a near constant warming trend of 0.04-0.05°C/decade was observed in all regions (**Figure 6**), suggesting widespread warming conditions throughout the adult Patagonian toothfish range in the Scotia Sea. However, we note caution when interpreting these trends as analyses of subsurface temperatures are based on model reanalysis (GLORYS12V1) and while this incorporates in-situ measurements, the corresponding outputs may be subject to shifting biases through time.

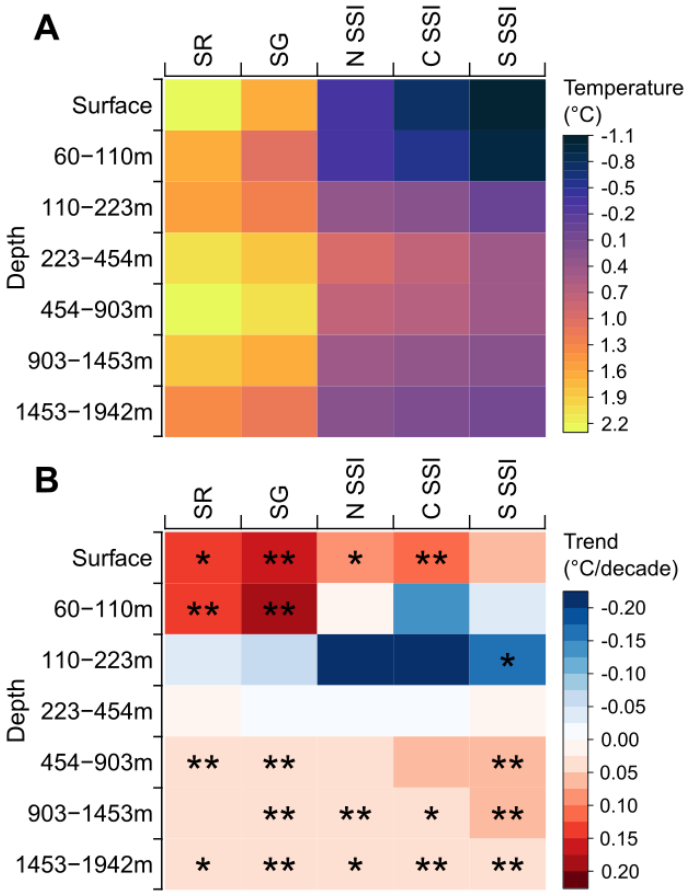

Figure 6. *Long-term average temperature (**A**) and trend estimates (**B**) for regions and depth-strata inhabited by Patagonian toothfish in the Scotia Sea. Average temperatures (**A**) represent the mean temperature from 1994-2023 within the 2000 m isobath in each region (Shag Rocks = 40-44°W, South Georgia = east of 40°W, N SSI = north of 57°S, C SSI = 57-58.1°S, S SSI = 58.2-60.5°S) at the stated depth range. Temperature trends (°C/decade; **B**) are from a linear model fitted to year-average temperatures for the same spatial (horizontal and vertical) and temporal extents as described in (**A**). Trend significance is shown as either * or **, based on whether the 90% (*) or 95% (**) confidence interval of the trend estimate didn't overlap with 0. All data were obtained from the Copernicus Marine Data Store, with sea surface temperature (SST) extracted from the Global Ocean OSTIA SST dataset, and remaining data extracted from the Global Ocean Physics Reanalysis dataset.*

Discussion

Ontogenetic shifts in distribution and association with environmental factors

Ontogenetic shifts in distribution are common in marine species (Wilbur, 1980; Bartolino et al., 2011; Barbeaux and Hollowed, 2018*),* with a bigger-deeper trend prevalent across multiple taxa (Macpherson and Duarte, 1991) and notably for demersal scavenging species such as Patagonian toothfish (Collins et al., 2005, 2010). While such shifts have long been recognised for Patagonian

toothfish (Collins et al., 2007), this study provides insights into their nature and timing together with potential environmental drivers.

The distribution of Patagonian toothfish measuring less than 37 cm suggested a preference for depths less than 200 m (< 26 cm) to 400 (26-37 cm) m. When combined with an apparent lower temperature limit (year-average conditions) of 1.8°C at the surface, or 1.2-1.4°C at 100 m depth, this resulted in a highly constrained predicted distribution, largely on the Shag Rocks shelf. A preference for shallower habitats in juvenile fish has been documented across multiple species (Gibson et al., 2002; Munsch et al., 2016; Perry et al., 2018) and may be associated with avoidance of predation risk, ontogenetic changes in foraging behaviour, or warmer temperatures (Sheaves et al., 2015). In general, fish larvae are assumed to be more temperature sensitive than juveniles or adults (Moyano et al., 2017). The association with temperature exhibited by the smallest size-classes of Patagonian toothfish may be a carry-over effect from larval development, with larvae seeking out or having higher survivability in warmer water. Recent analyses suggest that juvenile Patagonian toothfish abundance on the Shag Rocks shelf covaries with temperature during and following spawning, with lower abundance following cooler years (Cavanagh et al., 2025). This finding, coupled with our result that juvenile distribution has a strong relationship with temperature, suggests that temperature conditions may be most limiting during early development (Collin et al., 2021). As such, variability in environmental conditions may be magnified in terms of overall abundance of early life-stages through time (Cavanagh et al., 2025) as there are few other areas of suitable habitat to act as refugia if conditions are not optimal at this “hotspot”.

However, the temperature thresholds noted for juvenile Patagonian toothfish broadly correspond to the division between Shag Rocks and the South Georgia shelf, suggesting temperature may act as a proxy for underlying biogeographic (e.g. alternate prey) and/or other oceanographic (salinity, productivity) differences between the two areas. Notably, the ichthyofaunal assemblage on the South Georgia shelf is more diverse and contains relatively higher densities of predatory fish such as Scotia-

Sea icefish (*Chaenocephalus aceratus*) and South Georgia icefish (*Pseudochaenichthys georgianus*) (Belchier, 2013; Gregory et al., 2017), which may prey upon juvenile toothfish. In contrast, the smaller-bodied yellowfin notothen (*Patagonotothen guntheri*) dominate, and are restricted to, the Shag Rocks shelf and act as primary prey for juvenile toothfish (Collins et al., 2008). However, these differences are also likely tied to temperature, with yellowfin notothen occurring in warmer waters from the southern Patagonian shelf to Shag Rocks (Collins et al., 2008), and icefish species (apart from mackerel icefish, *Champsocephalus gunnari*, which inhabit both areas; Fallon et al., 2016) unable to withstand the warmer temperatures at Shag Rocks (Beers and Jayasundara, 2015).

Whilst the two smallest size-classes (< 26 cm, 26-37 cm) were predominantly caught on the Shag Rocks shelf, they were also captured in lower numbers on the South Georgia shelf, mainly in the nearshore environment (**Figure 2**). It is possible that juvenile toothfish are more abundant in shallow nearshore areas around South Georgia than suggested by our models, as these areas are largely unsuitable for trawl sampling. However, any associated bias regarding spatial distribution and relation to temperature is likely minimal given that larger size-classes, found at greater depths more accessible to trawl sampling, display similar temperature relationships (i.e., **Figure 2D**).

The relationship between abundance and SST or MWT was largely the same for sizes up to the 38-47 cm size-class, which all appeared to inhabit locations within a similar temperature range (SST > 1.8°C), prior to a shift to encompass a wider range of temperatures for larger sizes. As noted previously, we suspect this result for the smallest size-class is related to temperature conditions during early development, potentially guiding areas of suitable habitat. We posit that this relationship remains for fish in the next two size-classes (26-37 cm, 38-47 cm) because individuals appear to remain on the Shag Rocks shelf due to proximity to initial settlement grounds, rather than being a genuine reflection of sub-adult relationship with temperature. This supports other work that realized or observed thermal niches of marine organisms are potentially determined during early development (Drost et al., 2015; Collin et al., 2021). The weakening relationship with SST/MWT with increasing size (48-57 cm

size-class and upwards) is likely a direct consequence of downslope migration facilitating dispersal away from Shag Rocks to areas surrounding South Georgia given the deepwater canyon (>1500 m) separating the two areas, with only larger (older) fish migrating across. However, a preference for seafloor temperatures > 1.5°C, with an optimum of 2°C was also evident for the 38-47 cm and 48-57 cm size-classes (**Figure 2**). Whether this is an artefact of the depth range inhabited (seafloor temperatures typically increase up to a maximum of ~ 2°C at 600 m; **Figure 4**), or an attempt to remain within a specific temperature range is difficult to disentangle. For the largest size-class temperature effects were much reduced, aligning with the hypothesis that thermal ranges widen from early developmental stages through to adults (Dahlke et al., 2020; Collin et al., 2021).

Broad-scale distribution of adults in relation to seafloor temperature

Results from the longline fishery catch data from around South Georgia indicate limited influence of seafloor temperature on CPUE. This is not unexpected given that most areas in the depth range targeted by the fishery had seafloor temperatures between 1 and 2.5°C, therefore a lower temperature threshold may not occur within this region. In addition, because adult fish are vulnerable to longline fishing, the distribution of fish will be influenced by both the environment and fishing, and it may be harder to determine the influence of environmental effects, compared to the effects on the smaller fish caught in the groundfish survey. At SSI, Patagonian toothfish abundance declined rapidly below temperatures of 0.3°C, suggesting a threshold for adult Patagonian toothfish distribution (**Figure 5**). Whether this is a genuine temperature threshold is uncertain, as multiple non-exclusive hypotheses may give rise to the same latitudinal gradient in Patagonian toothfish CPUE along the SSI chain. The first is that an annual average temperature of 0.3°C represents the limit below which Patagonian toothfish are unable to sustain core functions, such as foraging and growth (Sandersfeld et al., 2017). This is consistent with the lack of antifreeze glycoproteins in Patagonian toothfish preventing them from occupying sub-zero temperatures (Miya et al., 2015). Whilst a physiological explanation is appealing, Patagonian toothfish have been captured throughout the SSI chain, albeit at much reduced

catch-rates in the south (i.e., **Figure 5**), suggesting that individuals are capable of persisting at lower temperatures, at least over short periods of time.

A second hypothesis is that the observed distribution is truncated due to the biogeographic boundary imposed by deep-water passages north and south of Saunders Island, which happen to coincide with the 0.3°C threshold (**Figure 5**). In both passages, temperature at depth is below 0°C and midwater current velocities are high, indicating that transit either near or above the seafloor may be prevented by temperature conditions (seafloor), transverse current velocity (midwater), or a combination thereof.

Finally, the distributional limit may be imposed by competition with Antarctic toothfish, which may also be mediated by ambient temperature conditions (Kordas et al., 2011). Longline fishery catch along the SSI chain transitions from Patagonian toothfish in the north, to Antarctic toothfish south of Saunders Island (Soeffker et al., 2022), indicating that Antarctic toothfish show the opposite trend in abundance to Patagonian toothfish. In contrast to Patagonian toothfish, Antarctic toothfish are a high-Antarctic species adapted to withstand sub-zero temperatures (Chen and Cheng, 1997), with a preferred temperature of -0.1 to 0.06°C across their range (Nissen et al., 2025). It is plausible that Antarctic toothfish exclude Patagonian toothfish under the colder conditions in the southern part of the SSI chain (and vice versa further north) and that the temperature threshold of 0.3°C is related to competitive balance between the two species. This is further supported by the observation that Antarctic toothfish have increased their range northward in the SSI over recent years (Soeffker et al., 2022; Hollyman, P.R. and Collins, M.A., pers. comm), coincident with a reduction in the Patagonian toothfish population (**Figure S13**), suggesting that Antarctic toothfish may occupy sub-optimal (i.e., warmer) habitats when there is reduced or absent competition from Patagonian toothfish. Taken further, this suggests that distributional limits of both species at SSI may be tied to pulses of Patagonian toothfish recruitment at South Georgia (Roberts, 2011; Barbeaux and Hollowed, 2018), with a more southerly boundary following periods of high recruitment and spill-over of juvenile Patagonian

toothfish to the SSI, followed by a gradual reduction in Patagonian toothfish and expansion of Antarctic toothfish between years of high Patagonian toothfish recruitment.

Whether the apparent temperature threshold found at SSI operates directly on Patagonian toothfish via physiological effects together with the presence of bathymetric boundaries, and/or indirectly, coupled with prey and predator assemblages or via an alteration to the competitive balance between Patagonian and Antarctic toothfish, necessitates further study.

Implications for fisheries management

Together, our analyses of the two datasets indicate a strong influence of depth and temperature on the spatial distribution of Patagonian toothfish and underscore the importance of life stage-specific habitat requirements and environmental thresholds in shaping overall distribution. Several key considerations emerge from these findings for fisheries management. Fisheries management often relies on fishery-dependent data focused on adults, which risks overlooking early-life bottlenecks or habitat constraints that influence population structure. Furthermore, evaluating only adult thermal niches risks underestimating vulnerability and missing critical early-life habitat. For instance, in this case, an analysis based solely on adult distribution and abundance would only yield the (potentially) lower thermal limit at SSI, without identifying the importance of Shag Rocks as a “thermal island” for juveniles. Yet this is key to understanding how distribution changes in the early years and points to areas that are important to focus on for recruitment and environmental sensitivity. Identifying and monitoring areas that are important for juvenile stages, especially those acting as thermal refuges, is critical for understanding recruitment dynamics and population resilience under climate change (Barceló et al., 2016; Stamp et al., 2025).

Integrating earlier life-stage information into management considerations where possible will improve forecasting and management. There is a need to improve knowledge of these stages, particularly eggs and larval stages for which little is known. Fisheries management will need to be flexible and responsive, particularly as climate change alters temperature regimes and habitat availability across

different regions and depths (Cavanagh et al., 2025), accounting for how such change will differentially affect each life stage and geographic area, rather than treating populations as environmentally homogenous.

Future change scenarios (next steps)

Several scenarios/hypotheses emerge from this work that will inform our future analyses of Patagonian toothfish distribution under climate change:

(i) *changing habitat availability for juvenile fish*: ocean warming could increase the extent of suitable habitat for juveniles in this region (**Figure 6**). Given the preference for shallow water exhibited by the smallest size class (**Figure 3**), this would only occur if warming affects the coastline. This is a realistic possibility, as shallow strata have shown the highest rates of surface warming over the past 30 years (**Figure 6**), and this trend appears to be continuing. Whether this manifests as distribution change depends on the mechanisms constraining juvenile distribution - e.g. predator-prey assemblages, and how those assemblages respond to warming (Ward et al., 2025).

(ii) *intermediate size-class dynamics*: distributional shifts for intermediate size-classes will most likely follow those exhibited by recruits. Although research suggests intermediate size-classes of fish are the most adaptable/mobile to changing conditions (Barbeaux and Hollowed 2018), in Patagonian toothfish the distribution of these size-classes is primarily limited by suitable habitat at depth given ontogenetic migration to deeper water, rather than by temperature surrounding South Georgia. It is feasible that warming conditions may influence the timing of ontogenetic movement, but not the overall distribution. In the SSI, warming has the potential to open up new habitat for sub-adults;

(iii) *changing habitat availability for adults*: warming at the SSI may increase habitat availability for Patagonian toothfish, but the extent of any distributional shift will depend on the mechanisms restricting their current distribution (thermal tolerance: increase in

habitat likely; biogeographic boundary: unlikely to change; thermally-mediated competition: habitat may increase but outcome dependent on how Antarctic toothfish respond to warming), as well as how warming affects recruitment elsewhere at South Georgia (Cavanagh et al., 2025). Given rates of warming at depth, tentatively estimated at 0.05°C/decade (**Figure 6**), any such changes will likely occur only over longer time-scales.

Conclusion

Due to data limitations, most analyses of thermal niches and associated spatial distributions in marine systems focus on adult life stages. This study on Patagonian toothfish underscores the importance of understanding temperature relationships across different developmental stages to capture species' environmental sensitivities and potential responses to climate change. Incorporating life-stage differences is essential for improving forecasts of distributional shifts and informing fisheries management. These findings further highlight the need for more data on early life stages, particularly eggs and larvae, including vertical distribution and patterns of retention and dispersal (Cavanagh et al., 2025).

Acknowledgements

We acknowledge the UK Government Darwin Plus Programme for funding this project, also the British Antarctic Survey (BAS) and Cefas for providing additional support. RC, MC, JF, SH, ST, CW were additionally supported by the BAS National Capability Antarctic Logistics and Infrastructure program "Research, Conservation and Leadership in Southern Ocean Ecosystems (CONSEC)", supported by the Natural Environment Research Council, a part of UK Research and Innovation. This study was conducted using E.U. Copernicus Marine Service Information (OSTIA sea surface temperature, https://doi.org/10.48670/moi-00165; GLORYS12V1 full depth temperature; https://doi.org/10.48670/moi-00021).

References

Abreu, J., Hollyman, P.R., Xavier, J.C., Bamford, C.C.G., Phillips, R.A., and Collins, M.A. 2024. Trends in population structure of Patagonian toothfish over 25 years of fishery exploitation at South Georgia. Fisheries Research, 279. 12 pp. 10.1016/j.fishres.2024.107122

Agnew, D.J., 2000. The illegal and unregulated fishery for toothfish in the Southern Ocean, and the CCAMLR catch documentation scheme. Marine Policy 24(5): 361-374. https://doi.org/10.1016/S0308-597X(00)00012-9

Arkhipkin, A.I., Brickle, P., Lee, B., Shaw, P.W., and McKeown, N.J. 2022. Taxonomic re-appraisal for toothfish (Dissostichus: Notothenioidea) across the Antarctic Polar Front using genomic and morphological studies. Journal of Fish Biology 100(5): 1158-1170. https://doi.org/10.1111/jfb.15013

Aschan, M., Fossheim, M., Greenacre, M., and Primicerio, R., 2013. Change in fish community structure in the Barents Sea. PLoS One, 8(4), p.e62748.

Azmi, K., Pilling, G., Bell, J., Chang, Y.-J., Dutilloy, A., Frawley, T. H., Hamer, P., Hampton, J., Hanich, Q., Hill-Moana, T., Hsu, J., Hurry, G., Knittweis, L., Lin, H., Lu, D., Neubauer, P., Nicol, S., Scott, R., Senina, I., Wang, Y., Williams, A. J., and Zhang, F. 2025. Putting Regional Fisheries Management Organisations' Climate Change House in Order. Fish and Fisheries. Advance online publication. https://doi.org/10.1111/faf.70015

Bamford, C., Hollyman, P.R., Abreu, J., Darby, C., and Collins, M.A. 2024. Spatial, temporal, and demographic variability in Patagonian toothfish (Dissostichus eleginoides) spawning from twenty-five years of fishery data at South Georgia. Deep-Sea Research Part I. 203, 104199. doi.org/10.1016/j.dsr.2024.104260

Bansemer, C.S., and Bennett, M.B., 2011. Sex-and maturity-based differences in movement and migration patterns of grey nurse shark, *Carcharias taurus*, along the eastern coast of Australia. Marine and Freshwater Research, 62(6): 596-606.

Barange, M., Bahri, T., Beveridge, M.C., Cochrane, K.L., Funge-Smith, S., and Poulain, F. 2018. Impacts of climate change on fisheries and aquaculture. United Nations' Food and Agriculture Organization, 12(4), pp.628-635.

Barbeaux, S.J., and Hollowed, A.B., 2018. Ontogeny matters: climate variability and effects on fish distribution in the eastern Bering Sea. Fisheries Oceanography, 27(1), pp.1-15. https://doi.org/10.1111/fog.12229

Barceló, C., Ciannelli, L., Olsen, E.M., Johannessen, T., and Knutsen, H. 2016. Eight decades of sampling reveal a contemporary novel fish assemblage in coastal nursery habitats. Global Change Biology 22: 1155– 1167. https://doi.org/10.1111/gcb.13047

Bartolino V, Ciannelli L, Bacheler NM, Chan KS. Ontogenetic and sex-specific differences in density-dependent habitat selection of a marine fish population. Ecology. 2011 Jan;92(1):189-200. doi: 10.1890/09-1129.1. PMID: 21560689.

Beaugrand, G., and Reid, P.C. 2003 Long-term changes in phytoplankton, zooplankton and salmon related to climate. Global Change Biology 9:801–817. https://doi.org/10.1046/j.1365-2486.2003.00632.x

Belchier, M. 2013. Decadal trends in the South Georgia demersal fish assemblage. CCAMLR Working Group on Fisheries Stock Assessment WG-FSA-2013/26

Belchier, M., and Collins, M.A. 2008. Environmental drivers of recruitment and growth variability in Patagonian toothfish (Dissostichus eleginoides) at South Georgia. Marine Biology. 155: 493-503. https://doi.org/10.1016/j.ecss.2021.107473

Belchier, M., Collins, M.A., Gregory, S., Hollyman, P., and Soeffker, M. 2022. From sealing to the MPA – A history of exploitation, conservation and management of marine living resources at the South Sandwich Islands. Deep Sea Research II, 198, 105056. https://doi.org/10.1016/j.dsr2.2022.105056

Beers, J.M., and Jayasundara, N. 2015. Antarctic notothenioid fish: what are the future consequences of 'losses' and 'gains' acquired during long-term evolution at cold and stable temperatures? The Journal of Experimental Biology, 218(12):1834-1845. https://doi.org/10.1242/jeb.116129

Bessell-Browne, P., Punt, A. E., Smith, D. C., et al. 2025. Incorporating Climate Change Impacts Within Harvest Strategies: An Overview of Approaches. Fish and Fisheries 26 (5): 942-956. https://doi.org/10.1111/faf.70010.

Bishop, J., 2006. Standardizing fishery-dependent catch and effort data in complex fisheries with technology change. Reviews in Fish Biology and Fisheries, 16(1): 21-38. http://dx.doi.org/10.1007/s11160-006-0004-9

Boucher, E.M., 2018. Disentangling reproductive biology of the Patagonian toothfish Dissostichus eleginoides: skipped vs obligatory annual spawning, foraging migration vs residential life style. Environmental Biology of Fishes 101 (9), 1343-1356. doi: 10.1007/s10641-018-0781-8

Boehme, L., Meredith, M.P., Thorpe, S.E., Biuw, M., and Fedak M. 2008. Antarctic Circumpolar Current frontal system in the South Atlantic: Monitoring using merged Argo and animal-borne sensor data. Journal Geophysical Research (113), C09012, doi:10.1029/2007JC004647

Brigden, K.E., Marshall, C.T., Scott, B.E., Young, E.F., and Brickle, P., 2017. Interannual variability in reproductive traits of the Patagonian toothfish Dissostichus eleginoides around the sub-Antarctic island of South Georgia. Journal of Fish Biology 91 (1), 278-301. doi: 10.1111/jfb.13344

Brigden, K. 2019. The reproductive ecology of Patagonian toothfish (Dissostichus eleginoides, Smitt 1898) around the sub-Antarctic island of South Georgia: spatial and temporal patterns and processes spanning two decades of data. PhD thesis. University of Aberdeen, UK.

Cavanagh, R.D., Trathan, P.N., Hill, S.L., Melbourne-Thomas, J., Meredith, M.P., Hollyman, P., Krafft, B.A., MC Muelbert, M., Murphy, E.J., Sommerkorn, M., Turner, J., and Grant, S.M. 2021. Utilising IPCC

assessments to support the ecosystem approach to fisheries management within a warming Southern Ocean. Marine Policy 131. https://doi.org/10.1016/j.marpol.2021.104589

Cavanagh, R., and Pardo, E. 2024. Progress with recommendations from the CCAMLR Workshop on Climate Change. CCAMLR Working Group on Fish Stock Assessment WG-FSA-2024/14.

Cavanagh, R.D., Jones, T., Thorpe, S.E, Cleeland, J., Earl, T., Freer, J.J, Hill, S.L., Hogg, O.T., Hollyman, P.R., Waluda, C.M., Collins, M.A. 2025. Temperature variation associated with interannual variability in abundance of juvenile Patagonian toothfish (*Dissostichus eleginoides*) at South Georgia. CCAMLR WG-FSA-2025/XX

Cavole, L.M., Demko. A.M., Diner, R.E. Giddings, A. Koester, I., Pagniello, C.M.L.S. Paulsen, M.-L., Ramirez-Valdez, A., Schwenck, S.M., Yen, N.K., Zill, M.E., and Franks, P.J.S. 2016. Biological impacts of the 2013–2015 warm-water anomaly in the Northeast Pacific: Winners, losers, and the future. Oceanography 29(2):273–285, http://dx.doi.org/10.5670/oceanog.2016.32.

Chen, L., DeVries, A. L., and Cheng, C. H. 1997. Evolution of antifreeze glycoprotein gene from a trypsinogen gene in Antarctic notothenioid fish. Proceedings of the National Academy of Sciences. USA 94: 3811–3816.

Collin, R., Rebolledo, A.P., Smith, E., and Chan, K.Y.K. 2021. Thermal tolerance of early development predicts the realized thermal niche in marine ectotherms. Functional Ecology, 35(8):1679-1692. https://doi.org/10.1111/1365-2435.13850

Collins, M.A., Bailey, D.M., Ruxton, G.D., and Priede, I.G. 2005. Trends in body size across an environmental gradient: a differential response in scavenging and non-scavenging demersal deep-sea fish. Proceedings of the Royal Society B 272, 2051-2057.

Collins, M.A., Ross, K., Belchier, M., and Reid, K., 2007. Distribution and diet of juvenile Patagonian toothfish on the South Georgia and Shag Rocks shelves (Southern Ocean). Marine Biology 152, 135-147. https://doi.org/10.1098/rspb.2005.3189

Collins, M.A., Shreeve, R.S., Fielding, S., and Thurston, M.H., 2008. Distribution, growth, diet and foraging behaviour of the yellow-fin notothen Patagonotothen guntheri (Norman) on the Shag Rocks shelf (Southern Ocean). Journal of Fish Biology, 72(1), pp.271-286. https://doi.org/10.1111/j.1095-8649.2007.01711.x

Collins, M.A., Brickle, P., Brown, J., and Belchier, M. 2010. The Patagonian toothfish: biology, ecology and fishery. Advances in Marine Biology, 58, 227-300. https://doi.org/10.1016/B978-0-12-381015-1.00004-6

Combes, V., Matano, R.P., Meredith, M.P., and Young, E.F. 2023. Variability of the shelf circulation around South Georgia, Southern Ocean. Journal of Geophysical Research: Oceans, 128 (2). 13 pp. 10.1029/2022JC019257

Constable, A.J., de la Mare, W.K., Agnew, D.J., Everson, I., and Miller, D. 2000. Managing fisheries to conserve the Antarctic marine ecosystem: practical implementation of the Convention on the Conservation of Antarctic Marine Living Resources (CCAMLR). ICES Journal of Marine Science 57, 778–791. https://doi.org/10.1006/jmsc.2000.0725

Cruz, L., Pennino, M., and Lopes, P. 2004. Fisheries track the future redistribution of marine species. Nature Climate Change 14:1093–1100 https://doi.org/10.1038/s41558-024-02127-7

Dahlke, Flemming & Wohlrab, Sylke & Butzin, Martin & Pörtner, Hans-Otto. (2020). Thermal bottlenecks in the life cycle define climate vulnerability of fish. Science. 369. 65-70. 10.1126/science.aaz3658.

Dormann, C.F., Calabrese, J.M., Guillera-Arroita, G., Matechou, E., Bahn, V., Bartoń, K., Beale, C.M., Ciuti, S., Elith, J., Gerstner, K., and Guelat, J. 2018. Model averaging in ecology: A review of Bayesian, information-theoretic, and tactical approaches for predictive inference. Ecological monographs, 88(4), pp.485-504. https://doi.org/10.1002/ecm.1309

Drost, H.E., Fisher, J., Randall, F., Kent, D., Carmack, E.C., Farrell, A.P. 2015. Upper thermal limits of the hearts of Arctic cod *Boreogadus saida*: adults compared with larvae. Journal of Fish Biology 88: 718–726. doi: 10.1111/jfb.12807

Dulvy, N.K., Rogers, S.I., Jennings, S., Stelzenmüller, V., Dye, S.R., and Skjoldal, H.R., 2008. Climate change and deepening of the North Sea fish assemblage: a biotic indicator of warming seas. Journal of Applied Ecology, 45(4): 1029-1039. https://doi.org/10.1111/j.1365-2664.2008.01488.x

Earl, T., Eleanor MacLeod, Marta Söffker, Nico Gasco, Félix Massiot-Granier, Paul Tixier, Christopher Darby. 2021. Whale depredation in the South Georgia Patagonian toothfish (Dissostichus eleginoides) fishery in the South Atlantic: a comparison of estimation methods. ICES Journal of Marine Science, Volume 78, Issue 10, December 2021, Pages 3817–3833, https://doi.org/10.1093/icesjms/fsab212

Earl, T., Readdy, L., Alewijnse, S., Devine, J., Dunn, A., Le Clech, R., Maschette, D., Masere, C., Massiot-Granier, F., Ouzoulias, F., Péron, C. Walker, N. and Ziegler, P. 2024. Approaches to projecting recruitment in toothfish assessment models. CCAMLR Working Group on Statistics, Assessments and Modelling WG-SAM-2024/23.

Earl, T., and Readdy, L. 2024. Assessment of Patagonian toothfish (*Dissostichus eleginoides*) in Subarea 48.3. CCAMLR Working Group on Fish Stock Assessment Paper WG-FSA-IMAF-2024/29.

Eastman, J.T. 1990. The biology and physiological ecology of notothenioid fishes. In: O. Gon, P.C. Heemstra (Eds.), Fishes of the Southern Ocean, J.L.B. Smith Institute of Ichthyology, Grahamstown (1990), pp. 34-51.

Ern, R., Andreassen, A.H., and Jutfelt, F., 2023. Physiological mechanisms of acute upper thermal tolerance in fish. Physiology, 38(3), pp.141-158. https://doi.org/10.1152/physiol.00027.2022

Everson, I., and Murray, A., 1999. Size at sexual maturity of Patagonian toothfish. CCAMLR Sci, 6, pp.37-46.

Fallon, N.G., Collins, M.A., Marshall, C.T., and Fernandes, P.G. 2016. Assessing consistency of fish survey data: uncertainties in the estimation of mackerel icefish (*Champsocephalus gunnari*) abundance at South Georgia. Polar Biology, 39(4), pp.593-603. https://link.springer.com/article/10.1007/s00300-015-1810-0

Gibson, R.N., Robb, L., Wennhage, H., and Burrows, M.T., 2002. Ontogenetic changes in depth distribution of juvenile flatfishes in relation to predation risk and temperature on a shallow-water nursery ground. Marine Ecology Progress Series, 229: 233-244. http://dx.doi.org/10.3354/meps229233

Gregory, S., Collins, M.A., and Belchier, M., 2017. Demersal fish communities of the shelf and slope of South Georgia and Shag Rocks (Southern Ocean). Polar Biology, 40(1), pp.107-121.

Hijmans, R. 2025. raster: Geographic Data Analysis and Modeling. R package version 3.6-31, <https://rspatial.org/raster>.

Hogg, O.T., Cavanagh, R.D, Grant, S., Belchier, M., Gregory, S., and Collins, M.A., 2021. Key climate change effects on the coastal and marine environment around the Polar UK Overseas Territories. Marine Climate Change Impacts Partnership Science Review. 0.14465/2021.orc02.pol

Hollowed, A.B., Barbeaux, S.J., Cokelet, E.D., Farley, E., Kotwicki, S., Ressler, P.H., Spital, C., and Wilson, C.D. 2012. Effects of climate variations on pelagic ocean habitats and their role in structuring forage fish distributions in the Bering Sea. Deep Sea Research Part II: Topical Studies in Oceanography, 65: 230-250. https://doi.org/10.1016/j.dsr2.2012.02.008

Hollyman, P.R., Hill, S.L., Laptikhovsky, V.V., Belchier, M., Gregory, S., Clement, A., Collins, M.A. 2021. A long road to recovery: dynamics and ecology of the marbled rockcod (Notothenia rossii, family: Nototheniidae) at South Georgia, 50 years after overexploitation. ICES Journal of Marine Science, 78(8): 2745-2756. https://doi.org/10.1093/icesjms/fsab150

Hollyman, P.R., Soeffker, M., Roberts, J., Hogg, O.T., Laptikhovsky, V.V., Queirós, J.P., Darby, C., Belchier, M., Collins, M.A. 2022. Bioregionalization of the South Sandwich Islands through community analysis of bathyal fish and invertebrate assemblages using fishery-derived data. Deep Sea Research Part II: Topical Studies in Oceanography, 198 (). 15 pp. 10.1016/j.dsr2.2022.105054

IPCC 2019. IPCC Special Report on the Ocean and Cryosphere in a Changing Climate [Portner, H.-O., Roberts, D.C., Masson-Delmotte, V., Zhai, P., Tignor, M., Poloczanska, E. et al., (eds.)], 2019. https://www.ipcc.ch/srocc/

IPCC 2022. Climate Change 2022: Impacts, Adaptation and Vulnerability. Contribution of Working Group II to the Sixth Assessment Report of the Intergovernmental Panel on Climate Change (Eds. H.-O. Pörtner, et al.,) (IPCC, Geneva, 2022).

Kordas, R.L., Harley, C.D., and O'Connor, M.I. 2011. Community ecology in a warming world: the influence of temperature on interspecific interactions in marine systems. Journal of Experimental Marine Biology and Ecology, 400(1-2), pp.218-226. https://doi.org/10.1016/j.jembe.2011.02.029

Lellouche, J. M., Greiner, E., Bourdalle-Badie, R., Garric, G., Melet, A., Drevillon, M., et al. (2021). The Copernicus Global 1/12° Oceanic and Sea Ice GLORYS12 Reanalysis. Frontiers in Earth Science, 9, Article ID: 698876. https://doi.org/10.3389/feart.2021.698876

Macpherson, E., and Duarte, C.M., 1991. Bathymetric trends in demersal fish size: is there a general relationship? Marine Ecology Progress Series, pp.103-112. http://doi.org/10.3354/meps071103

Masere, C., Le Clech, R., Alewijnse, S., Devine, J., Dunn, A., Earl, T., Maschette, D., Massiot-Granier, F., Ouzoulias, F., Péron, C., Readdy, L., Walker, N., and P. Ziegler. 2024a. Consideration of the impact of tagging and recapture effort on mark-recapture abundance estimators within integrated Casal2 stock assessments. CCAMLR Working Group on Statistics, Assessments and Modelling WG-SAM-2024/22

Masere, C., Le Clech, R., Alewijnse, S., Devine, J., Dunn, A., Earl, T., Maschette, D., Massiot-Granier, F., Ouzoulias, F., Péron, C., Readdy, L., Walker, N., and P. Ziegler. 2024b. Consideration of the impact of tagging and recapture effort on mark-recapture abundance estimators within integrated Casal2 stock assessments – supplementary material. CCAMLR Working Group on Statistics, Assessments and Modelling WG-SAM-2024/24

Melbourne-Thomas, J., Audzijonyte, A., Brasier, M.J. et al. 2022. Poleward bound: adapting to climate-driven species redistribution. Reviews in Fish Biology and Fisheries 32:231–251. https://doi.org/10.1007/s11160-021-09641-3

Meredith, M.P., Brandon, M.A., Murphy, E.J., Trathan, P.N., Thorpe, S.E., Bone, D.G., Chernyshkov, P. P., and Sushin, V.A. 2005. Variability in hydrographic conditions to the east and northwest of South Georgia, 1996–2001. Journal of Marine Systems, 53 (1-4): 143-167. doi:10.1016/j.jmarsys.2004.05.005

Murphy, E.J., Trathan, P.N., Watkins, J.L., Reid, K., Meredith, M.P., Forcada, J., Thorpe, S.E., Johnston, N.M., and Rothery, P. 2007. Climatically driven fluctuations in Southern Ocean ecosystems. Proceedings of the Royal Society B: Biological Sciences, 274 (). pp. doi:10.1098/rspb.2007.1180

Miya, T., Gon, O., Mwale, M., and Cheng, C.H.C., 2015. Multiple independent reduction or loss of antifreeze trait in low Antarctic and sub-Antarctic notothenioid fishes. Antarctic Science, 28(1):17-28. https://doi.org/10.1017/S0954102015000413

Moyano, M., Candebat, C., Ruhbaum, Y., Álvarez-Fernández, S., Claireaux, G., Zambonino-Infante, J.L., Peck, M.A. Effects of warming rate, acclimation temperature and ontogeny on the critical thermal maximum of temperate marine fish larvae. 2017. PLoS One. Jul 27;12(7):e0179928. doi: 10.1371/journal.pone.0179928. PMID: 28749960; PMCID: PMC5531428.

Mueter, F.J., and Litzow, M.A., 2008. Sea ice retreat alters the biogeography of the Bering Sea continental shelf. Ecological Applications, 18(2), pp.309-320. https://doi.org/10.1890/07-0564.1

Munsch, S., Cordell, J., and Toft, J. 2016. Fine-scale habitat use and behavior of a nearshore fish community: Nursery functions, predation avoidance, and spatiotemporal habitat partitioning. Marine Ecology Progress Series. 557. 10.3354/meps11862.

Neubauer, P., Andersen, K.H. 2019. Thermal performance of fish is explained by an interplay between physiology, behaviour and ecology. Conservation Physiology, Jun 10;7(1):coz025. doi: 10.1093/conphys/coz025

Nissen, C., Caccavo, J.A., and Morée, A.L. 2025. Twenty-First-Century Environmental Change Decreases Habitat Overlap of Antarctic Toothfish (*Dissostichus mawsoni*) and Its Prey. Global Change Biology, 31(2), p.e70063.

North, A.W. 2002. Larval and juvenile distribution and growth of Patagonian toothfish around South Georgia. Antarctic Science 14, Issue 1. doi.org/10.1017/S0954102002000548

NOAA National Centers for Environmental Information. 2022. ETOPO 2022 15 Arc-Second Global Relief Model. NOAA National Centers for Environmental Information. DOI: 10.25921/fd45-gt74.

Ouzoulias, F., Massiot-Granier, F., Alewijnse, S., Devine, J., Dunn, A., Earl, T., Le Clech, R., Maschette, D., Masere, C., Péron, C., Readdy, L., Walker, N. and Ziegler, P. 2024. Effects of implementing dynamic B0 in toothfish fisheries. CCAMLR Working Group on Statistics, Assessments and Modelling WG-SAM-2024/25.

Park, Y.-H, and Durand, I. 2019. Altimetry-derived Antarctic Circumpolar Current fronts. SEANOE. https://doi.org/10.17882/59800

Perry, D., Staveley, T.A.B., and Gullström, M. 2018. Habitat Connectivity of Fish in Temperate Shallow-Water Seascapes. Frontiers in Marine Science. 4:440. doi: 10.3389/fmars.2017.00440

Pinheiro, J., Bates, D. 2025. nlme: Linear and Nonlinear Mixed Effects Models. R package version 3.1-167, https://CRAN.R-project.org/package=nlme.

Pinsky, M.L., Worm, B., Fogarty, M.J., Sarmiento, J.L., and Levin, S.A. 2013. Marine taxa track local climate velocities. Science 341: 1239–1242. https://doi.org/10.1126/science.1239352

Pörtner, H.O., Peck, L., and Somero, G., 2007. Thermal limits and adaptation in marine Antarctic ectotherms: an integrative view. Philosophical Transactions of the Royal Society B: Biological Sciences, 362(1488), pp.2233-2258.

Roberts, J., Xavier, J.C., and Agnew, D.J. 2011. The diet of toothfish species *Dissostichus eleginoides* and *Dissostichus mawsoni* with overlapping distributions. Journal of Fish Biology 79(1):138-54. doi: 10.1111/j.1095-8649.2011.03005.x.

Rogers, A.D., Morley, S., Fitzcharles, E., Jarvis, K., and Belchier, M. 2006. Genetic structure of Patagonian toothfish (Dissostichus eleginoides) populations on the Patagonian shelf and Atlantic and western Indian ocean sectors of the Southern Ocean. Mar. Biol. 149, 915–924. https://doi.org/10.1007/s00227-006-0256-x

Sandersfeld, T., Mark, F.C., and Knust, R., 2017. Temperature-dependent metabolism in Antarctic fish: do habitat temperature conditions affect thermal tolerance ranges? Polar Biology, 40, pp.141-149. https://link.springer.com/article/10.1007/s00300-016-1934-x

SC-CAMLR-42. 2023. Report of the Forty-Second Meeting of the Scientific Committee, Hobart, Australia 16 – 20 October 2023. https://meetings.ccamlr.org/system/files/meeting-reports/e-sc-42-rep.pdf

Shaw, P.W., Arkhipkin, A.I., and Al-Khairulla, H. 2004. Genetic structuring of Patagonian toothfish populations in the Southwest Atlantic Ocean: the effect of the Antarctic Polar Front and deep-water troughs as barriers to genetic exchange. Molecular Ecology 13 (11), 3293–3303. https://doi.org/10.1111/j.1365-294x.2004.02327.x

Sheaves, M., Baker, R., Nagelkerken, I. et al. 2015. True Value of Estuarine and Coastal Nurseries for Fish: Incorporating Complexity and Dynamics. Estuaries and Coasts 38: 401–414. https://doi.org/10.1007/s12237-014-9846-x

Soeffker, M., Hollyman, P.R., Collins, M.A., Hogg, O.T., Riley, A., Laptikhovsky, V., Earl, T., Roberts, J., MacLeod, E., Belchier, M., and Darby, C. 2022. Contrasting life-history traits of two toothfish (Dissostichus spp.) species at their range edge around the South Sandwich Islands. Deep Sea Research Part II: Topical Studies in Oceanography 201, 105098. doi: 10.1016/j.dsr2.2022.105098

Stamp, T., West, E., Stewart, J.E., Plenty, S., Robbins, T., Sheehan, E. 2025. Effective protection of essential fish habitat requires understanding fish spatial ecology - lessons learnt from protected European bass nursery areas. ICES Journal of Marine Science, 82(4) https://doi.org/10.1093/icesjms/fsaf035

Sunday, J., Bates, A., and Dulvy, N.K. 2012. Thermal tolerance and the global redistribution of animals. Nature Climate Change 2:686–690. https://doi.org/10.1038/nclimate1539

Thorpe, S.E., and Murphy, E.J. 2022. Spatial and temporal variability and connectivity of the marine environment of the South Sandwich Islands, Southern Ocean. Deep Sea Research Part II: Topical Studies in Oceanography, 198 105057. 16 pp. 10.1016/j.dsr2.2022.105057

Thorson, J.T., 2019. Measuring the impact of oceanographic indices on species distribution shifts: The spatially varying effect of cold-pool extent in the eastern Bering Sea. Limnology and Oceanography, 64(6): 2632-2645. https://doi.org/10.1002/lno.11238

Townhill, B. L., Couce, E., Tinker, J., Kay, S., and Pinnegar, J.K. 2023. Climate change projections of commercial fish distribution and suitable habitat around north western Europe. Fish and Fisheries, 24: 848–862. https://doi.org/10.1111/faf.12773

Ward, D., Hill, N., Melbourne-Thomas, J., Welsford, D., Arangio, R., McNeill, M., Wotherspoon, S., Ziegler, P., and Corney, S. 2025. Exploring mechanisms of change in a Southern Ocean fishery with a co-produced network model. ICES Journal of Marine Science. 82. 10.1093/icesjms/fsaf095.

Welsford, D. 2023. Summary and Recommendations from Independent review of CCAMLR toothfish assessments, 2023. SC-CAMLR-42/02 Rev. 2

Whitehouse, M.J., Meredith, M.P., Rothery, P., Atkinson, A., Ward, P., and Korb, R.E. (2008) Rapid warming of the ocean around South Georgia, Southern Ocean, during the 20th century: Forcings, characteristics and implications for lower trophic levels. Deep-Sea Research Part I, 55 (10), 1218-1228. doi:10.1016/j.dsr.2008.06.002

Wilbur, H.M., 1980. Complex life cycles. Annual review of Ecology and Systematics, 11, pp.67-93.

Wood, S.N. 2011. Fast stable restricted maximum likelihood and marginal likelihood estimation of semiparametric generalized linear models. Journal of the Royal Statistical Society (B) 73(1):3-36. https://doi.org/10.1111/j.1467-9868.2010.00749.x

WG-FSA-IMAF-2024. Report of the Working Group on Fish Stock Assessment and Incidental Mortality Associated with Fishing. Hobart, Australia, 30 September to 11 October 2024. https://meetings.ccamlr.org/en/sc-camlr-43/14

Supplementary materials

Section 1: Additional information on groundfish survey data

Table S1. *Summary of bottom-trawl surveys used in analyses of Patagonian toothfish (Dissostichus eleginoides) distribution. All values presented are after data-cleaning and represent sample sizes entering analyses. Design abbreviations: SRS = stratified random sample, RAD = radial, DW = deepwater trawl surveys.*

Survey	Date start	Date end	Gear	Design	Trawls
SG87	29-Nov-86	17-Dec-86	B-454 OT	SRS	104
SG88	19-Dec-87	12-Jan-88	P32/36 OT	SRS	112
SG89	1-Feb-89	14-Feb-89	P32/36 OT	SRS	55
SG90	6-Jan-90	26-Jan-90	HC120 OT	SRS	68
SG91	22-Jan-91	11-Feb-91	FP120	SRS	77
SG92	3-Jan-92	26-Jan-92	FP120	SRS	81
SG94	4-Jan-94	8-Feb-94	FP120	SRS	81
SG97	2-Sep-97	29-Sep-97	FP120	SRS	55
SG00	16-Jan-00	30-Jan-00	FP120	SRS	41
SG02	12-Jan-02	1-Feb-02	FP120	SRS	63
SG03	7-Jan-03	31-Jan-03	FP120	RAD	38
SG04	7-Jan-04	5-Feb-04	FP120	SRS	64
SG05	7-Jan-05	25-Jan-05	FP120	SRS	42
SG06	3-Jan-06	1-Feb-06	FP120	SRS	66
SG07	27-Aug-07	21-Sep-07	FP120	SRS	49
SG08	16-Apr-08	30-Apr-08	FP120	SRS	70
SG09	15-Jan-09	23-Jan-09	FP120	SRS	73
SG10	15-Jan-10	24-Jan-10	FP120	SRS	75
DW10	29-Jan-10	31-Jan-10	FP120	DW	6
SG11	26-Jan-11	6-Feb-11	FP120	SRS	87
SG12	26-Jan-12	29-Jan-12	FP120	SRS[a]	22
SG13	22-Jan-13	29-Jan-13	FP120	SRS	68
SG15	13-Jan-15	23-Jan-15	FP120	SRS	77
SG17	30-Jan-17	7-Feb-17	FP120	SRS	72
DW19	5-Feb-19	5-Feb-19	FP120	DW	3
SG19	27-Jan-19	5-Feb-19	FP120	SRS	73
SG21	8-May-21	28-May-21	FP120	SRS	76
SG23	1-Feb-23	10-Feb-23	FP120	SRS	75

a: 2012 survey was incomplete, with sampling only on Shag Rocks and the NW South Georgia shelf

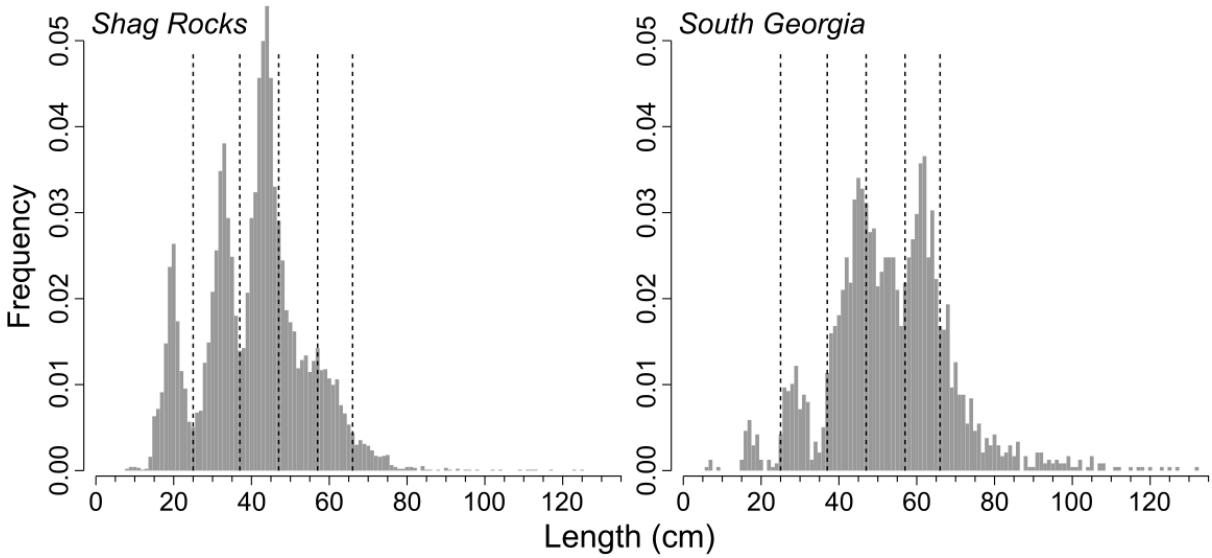

Figure S1. *Size-frequency distributions of Patagonian toothfish (Dissostichus eleginoides) captured during groundfish survey trawls on the Shag Rocks and South Georgia shelf systems. Vertical dashed lines indicate size-class cut-offs used throughout analyses of toothfish distribution at South Georgia.*

Section 2: Additional information on longline fishery data

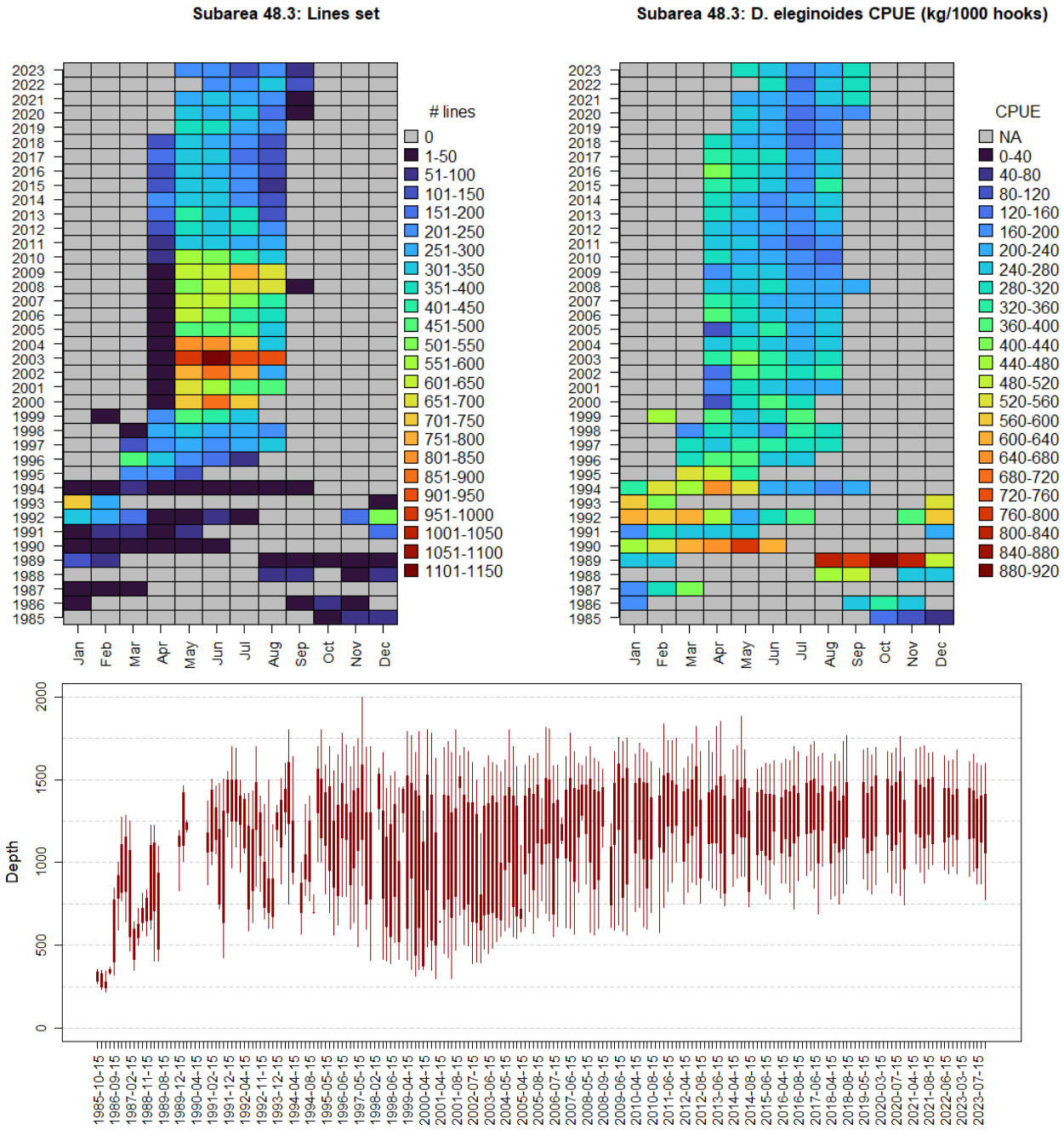

Figure S2. *Monthly summaries of fishing effort (number of lines set), catch-per-unit-effort (CPUE: kg per 1000 hooks) and depth distribution from longline fishery data in Subarea 48.3: South Georgia and Shag Rocks. Depth distributions are plotted as the interquartile (thick lines) and 90% range (thin lines).*

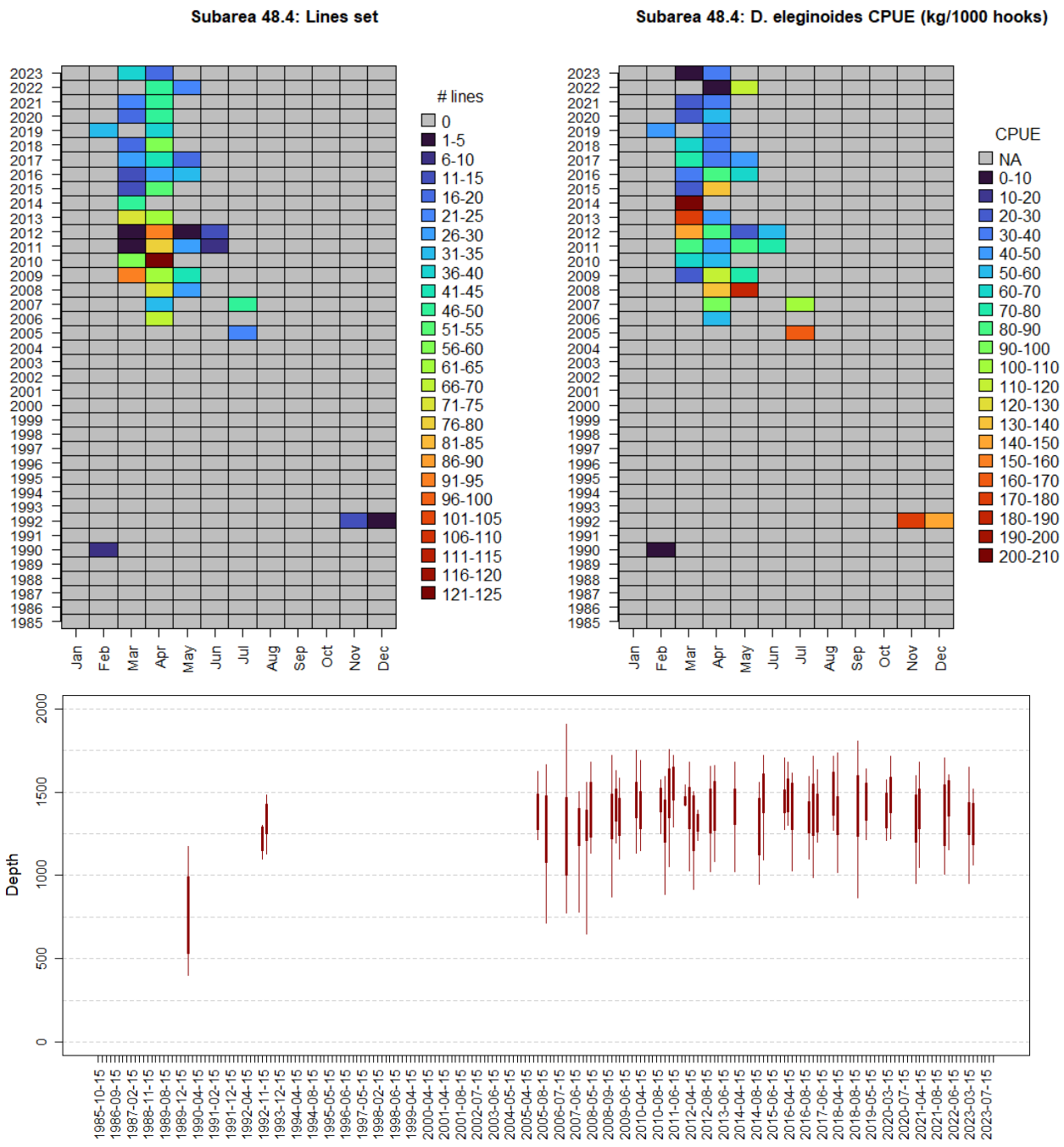

Figure S3. *Monthly summaries of fishing effort (number of lines set), catch-per-unit-effort (CPUE: kg per 1000 hooks) and depth distribution from longline fishery data in Subarea 48.4: South Sandwich Islands. Depth distributions are plotted as the interquartile (thick lines) and 90% range (thin lines).*

Section 3: Additional results for size-class distribution models

Collinearity of habitat covariates

Table S2. *Correlation coefficients between environmental covariates prepared for, and used in, development of Patagonian toothfish size-class distribution models. Correlations are coloured according to correlation strength (red = positive, blue = negative), and correlation coefficients with absolute values greater than 0.6 are given in bold font. Variable names are also formatted to indicate variables included in model development (bold font) and those dropped prior to model development (italics).*

Correlation coef (r)	**depth**	**slope**	**curve**	**CHL_mean**	*CHL_sd*	**MLT_mean**	*MLT_sd*	**SSAL_mean**	**SSAL_sd**	**FSAL_mean**	**FSAL_sd**	**VEL_mean**	*VEL_sd*	**SST_mean**	*SST_sd*	**SFT_mean**	*SFT_sd*	**MWT_mean**
depth																		
slope	33																	
curve	3	-6																
CHL_mean	4	-8	-3															
CHL_sd	9	10	10	**91**														
MLT_mean	-17	-38	8	-48	-40													
MLT_sd	-17	-22	22	-55	-37	**81**												
SSAL_mean	8	32	4	**-77**	-58	22	45											
SSAL_sd	-11	-32	-16	-8	-30	-18	-9	8										
FSAL_mean	**65**	45	-8	15	18	-38	-43	0	-15									
FSAL_sd	-55	-48	-5	0	-13	27	10	-26	18	**-73**								
VEL_mean	40	42	1	-36	-35	-24	-23	28	-7	47	-39							
VEL_sd	42	58	2	-20	-17	-40	-34	25	-14	50	-47	**92**						
SST_mean	-6	10	35	-16	13	17	55	31	-20	-19	-18	-17	-13					
SST_sd	13	23	30	-56	-26	35	57	**62**	-25	-1	-29	22	18	**84**				
SFT_mean	51	57	14	-19	6	-13	2	36	-35	**67**	**-67**	38	43	37	47			
SFT_sd	**-64**	-55	-10	2	-13	27	17	-22	28	**-87**	**79**	-42	-46	-13	-27	**-80**		
MWT_mean	-12	22	33	-46	-15	36	**70**	52	-29	-30	-11	-3	-1	**89**	**78**	37	-6	

Cross-validation

Predictive measures for toothfish distribution models were calculated through cross-validation, where models were fitted to a reduced dataset (90% of observations) and then tested against the observations in the held-out data. Firstly, observations (trawls) were labelled as one of 1-10 using a stratified random approach, such that strata were equally represented in each subset 1 through 10. Strata (n = 15) were based on combinations of depth zone, consisting of 3 levels of < 200m, 200-300 m and > 300 m, and sector consisting of Shag Rocks and division of the South Georgia shelf into northwest, northeast, southeast and southwest quadrants. Training datasets were constructed by selecting data corresponding to nine of the ten data labels, and the remaining data was assigned as the test dataset held back from model fitting. A model was fitted to the training dataset, and then applied to make predictions to the test dataset.

To quantify relative predictive error we used a likelihood-based score (Dormann et al. 2018). For each cross-validation iteration we calculate the log-likelihood of the data in the held-out data given predictions from the model trained on the remaining data:

$$\mathcal{L}_{CV}^{m} = \sum_{j=1}^{j=10} \ell\left(\boldsymbol{y_j} | \, \hat{\boldsymbol{y}}_{\boldsymbol{y}_{[-j]}}^{\boldsymbol{m}}, \hat{\theta}_{y_{[-j]}}^{m}\right)$$

Where $\mathcal{L}_{CV}^{m}$ is the likelihood score summed across folds, *j*, for a specific model, *m*, and $\ell\left(\boldsymbol{y_j} | \, \hat{\boldsymbol{y}}_{\boldsymbol{y}_{[-j]}}^{\boldsymbol{m}}, \hat{\theta}_{y_{[-j]}}^{m}\right)$ is the log-likelihood of observations $\boldsymbol{y_j}$ in the held-out data given predicted values $\hat{\boldsymbol{y}}_{\boldsymbol{y}_{[-j]}}^{\boldsymbol{m}}$ and negative binomial dispersion parameter, $\hat{\theta}_{y_{[-j]}}^{m}$, from the model fitted to data excluding fold *j* (indicated by $\boldsymbol{y}_{[-j]}$). For each iteration, the likelihood score was converted to a ratio, *D*, representing the relative improvement in cross-validated log-likelihood compared to a null model relative to the same difference calculated for a saturated model where all variability is explained:

$$D_{CV}^{m} = \frac{\mathcal{L}_{CV}^{0} - \mathcal{L}_{CV}^{m}}{\mathcal{L}_{CV}^{0} - \mathcal{L}_{CV}^{s}}$$

Where $\mathcal{L}_{CV}^{0}$ is the likelihood score for a model that only contains survey and area offset terms, and therefore accounts for effort and interannual differences in abundance but explains no spatial variability (i.e., null model), and $\mathcal{L}_{CV}^{s}$ is the likelihood score of a saturated model where predictions for each observation are set equal to their observed value and therefore explains all possible variation. When calculating $\mathcal{L}_{CV}^{s}$ the negative binomial dispersion parameter $\hat{\theta}$ was set to a high value of 1×10^{6} given that the best possible fit would be accompanied by lowest residual variance (negative binomial variance scales as $\mu + \mu^2/\theta$). The resulting predictive deviance score, D_{CV}^{m}, therefore ranges from 0 to 1, with 0 indicating predictions perform no better than the null in predicting spatial variability, and 1 indicating that predictions replicate the observed spatial variability perfectly.

Distribution model outputs

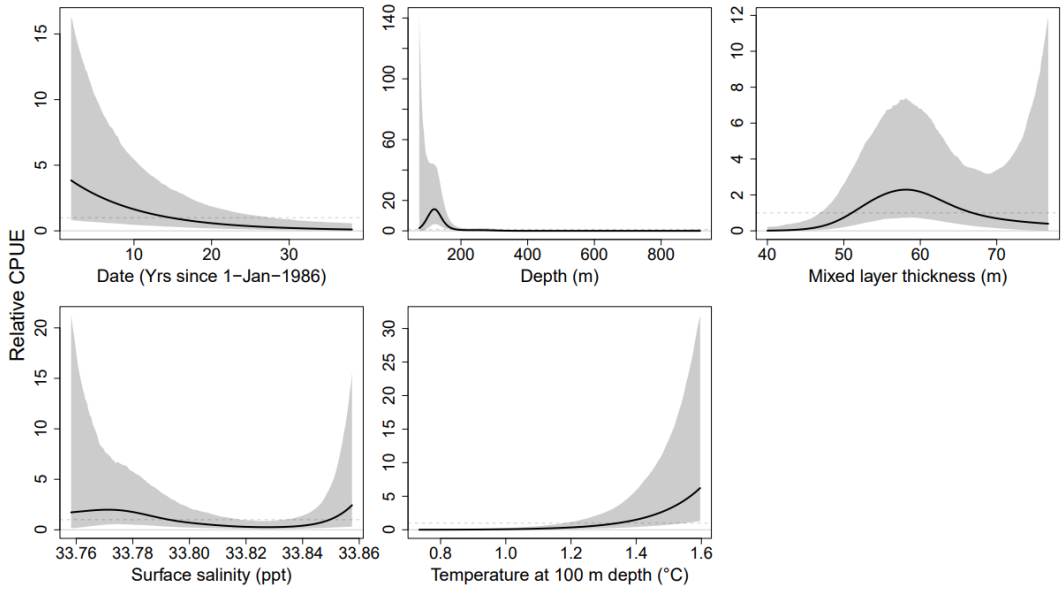

Figure S4. *Fitted relationships in the best model for < 26 cm Patagonian toothfish distribution around South Georgia. Values on the y-axis are relative CPUE, equal to model predicted values divided by the mean of those*

predictions across the covariate range, holding all other covariates constant. Lines and shading represent the mean and 95% confidence interval of fitted values, respectively.

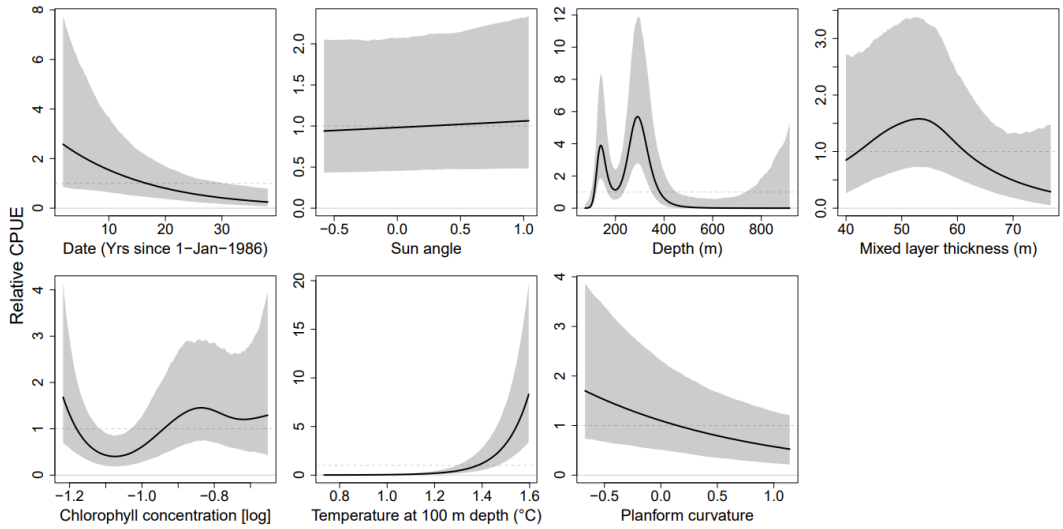

Figure S5. *Fitted relationships in the best model for 26-37 cm Patagonian toothfish distribution around South Georgia. Values on the y-axis are relative CPUE, equal to model predicted values divided by the mean of those predictions across the covariate range, holding all other covariates constant. Lines and shading represent the mean and 95% confidence interval of fitted values, respectively.*

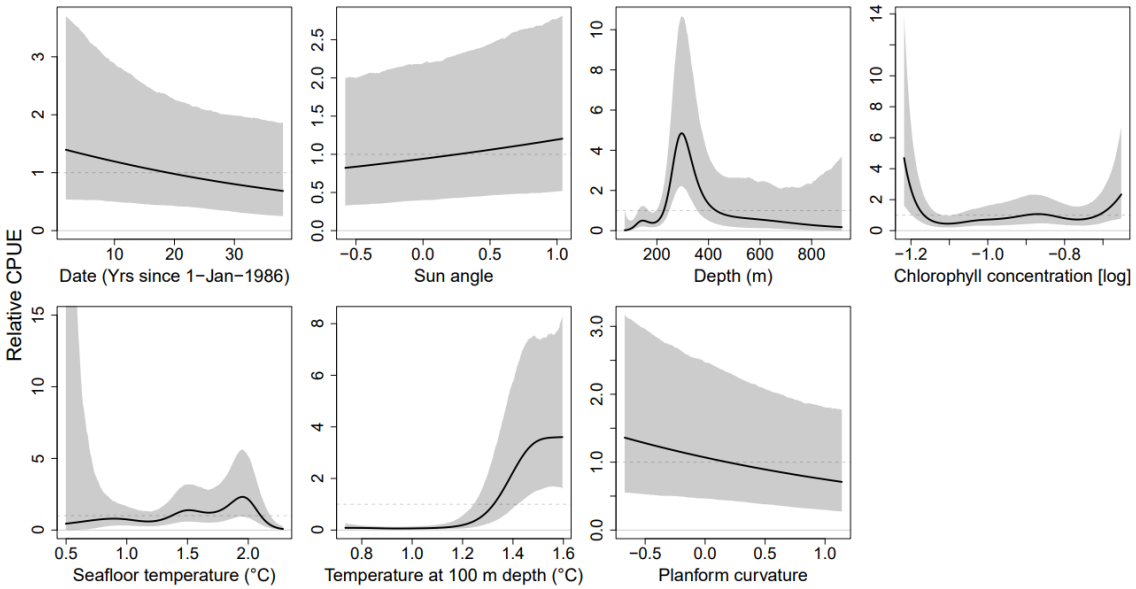

Figure S6. *Fitted relationships in the best model for 38-47 cm Patagonian toothfish distribution around South Georgia. Values on the y-axis are relative CPUE, equal to model predicted values divided by the mean of those predictions across the covariate range, holding all other covariates constant. Lines and shading represent the mean and 95% confidence interval of fitted values, respectively.*

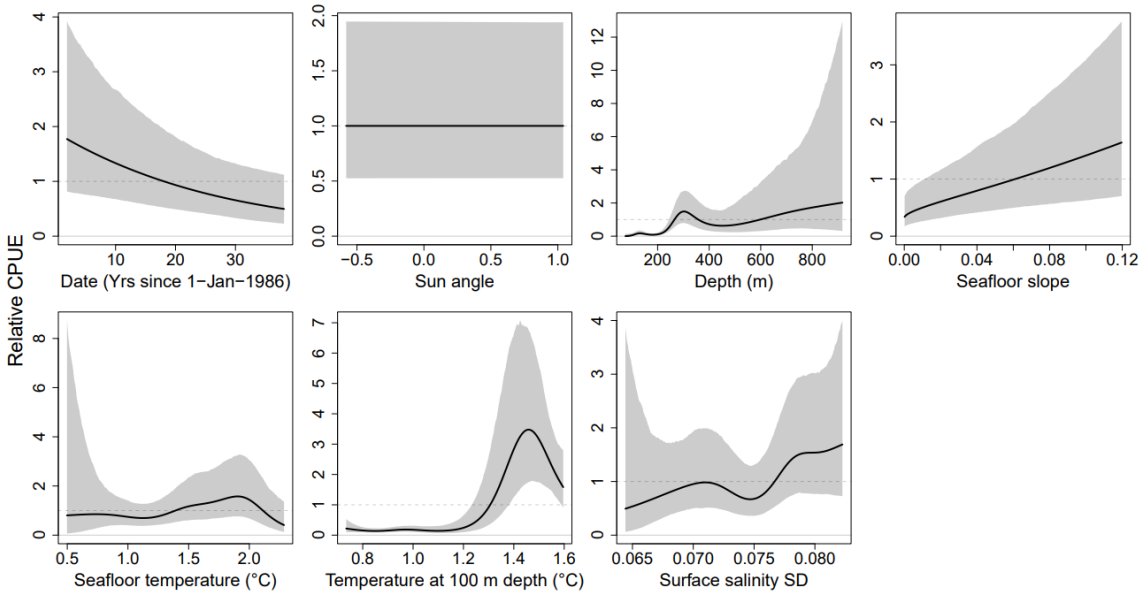

Figure S7. *Fitted relationships in the best model for 48-57 cm Patagonian toothfish distribution around South Georgia. Values on the y-axis are relative CPUE, equal to model predicted values divided by the mean of those predictions across the covariate range, holding all other covariates constant. Lines and shading represent the mean and 95% confidence interval of fitted values, respectively.*

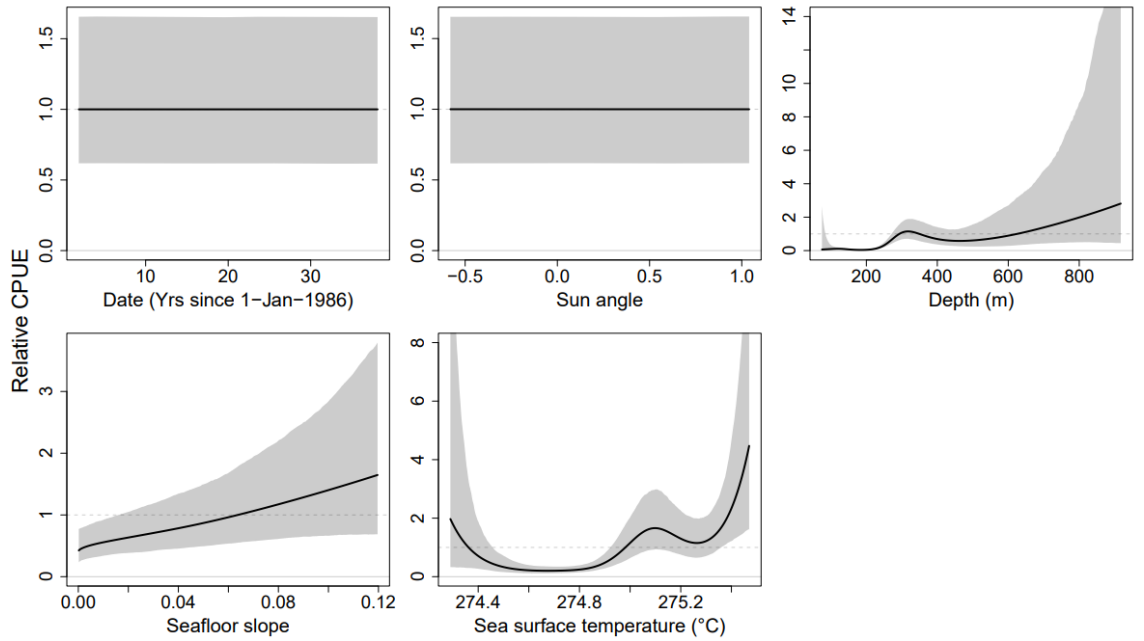

Figure S8. *Fitted relationships in the best model for 58-66 cm Patagonian toothfish distribution around South Georgia. Values on the y-axis are relative CPUE, equal to model predicted values divided by the mean of those predictions across the covariate range, holding all other covariates constant. Lines and shading represent the mean and 95% confidence interval of fitted values, respectively.*

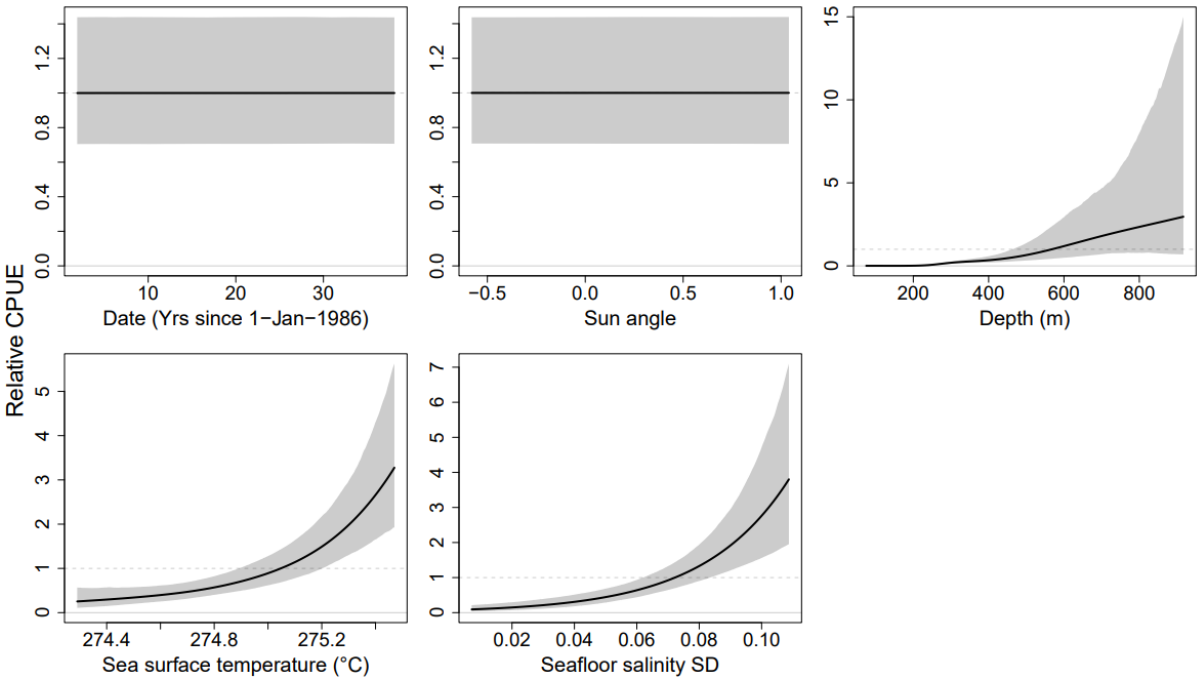

Figure S9. *Fitted relationships in the best model for > 66 cm Patagonian toothfish distribution around South Georgia. Values on the y-axis are relative CPUE, equal to model predicted values divided by the mean of those predictions across the covariate range, holding all other covariates constant. Lines and shading represent the mean and 95% confidence interval of fitted values, respectively.*

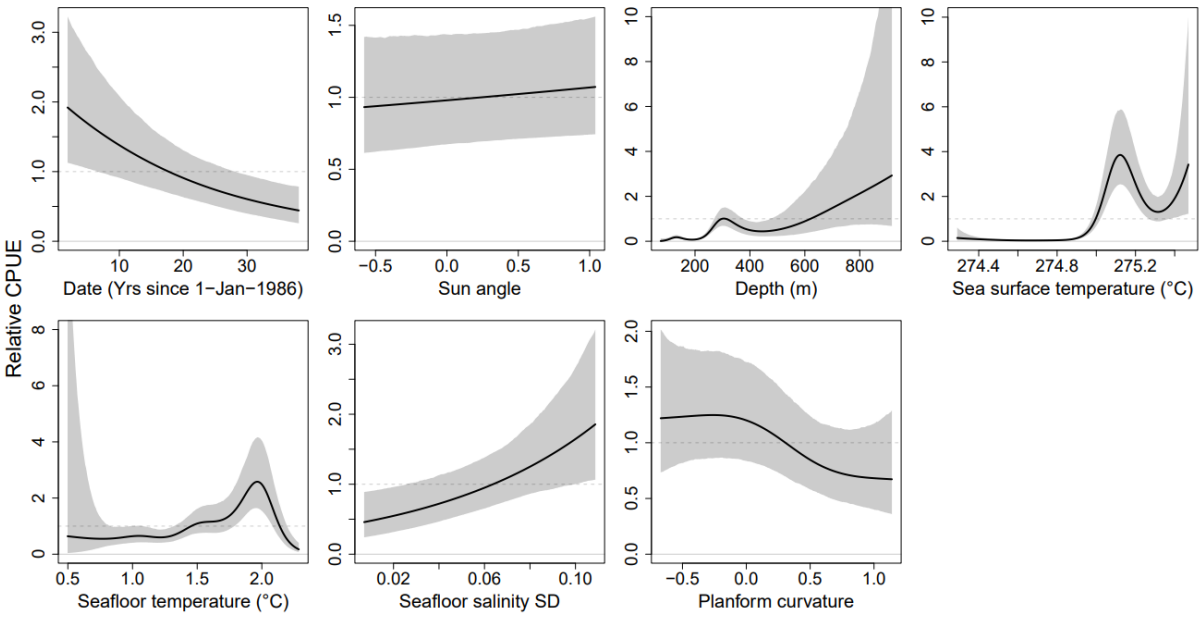

Figure S10. *Fitted relationships in the best model for Patagonian toothfish distribution, irrespective of size-class, around South Georgia. Values on the y-axis are relative CPUE, equal to model predicted values divided by the mean of those predictions across the covariate range, holding all other covariates constant. Lines and shading represent the mean and 95% confidence interval of fitted values, respectively.*

Prediction uncertainty

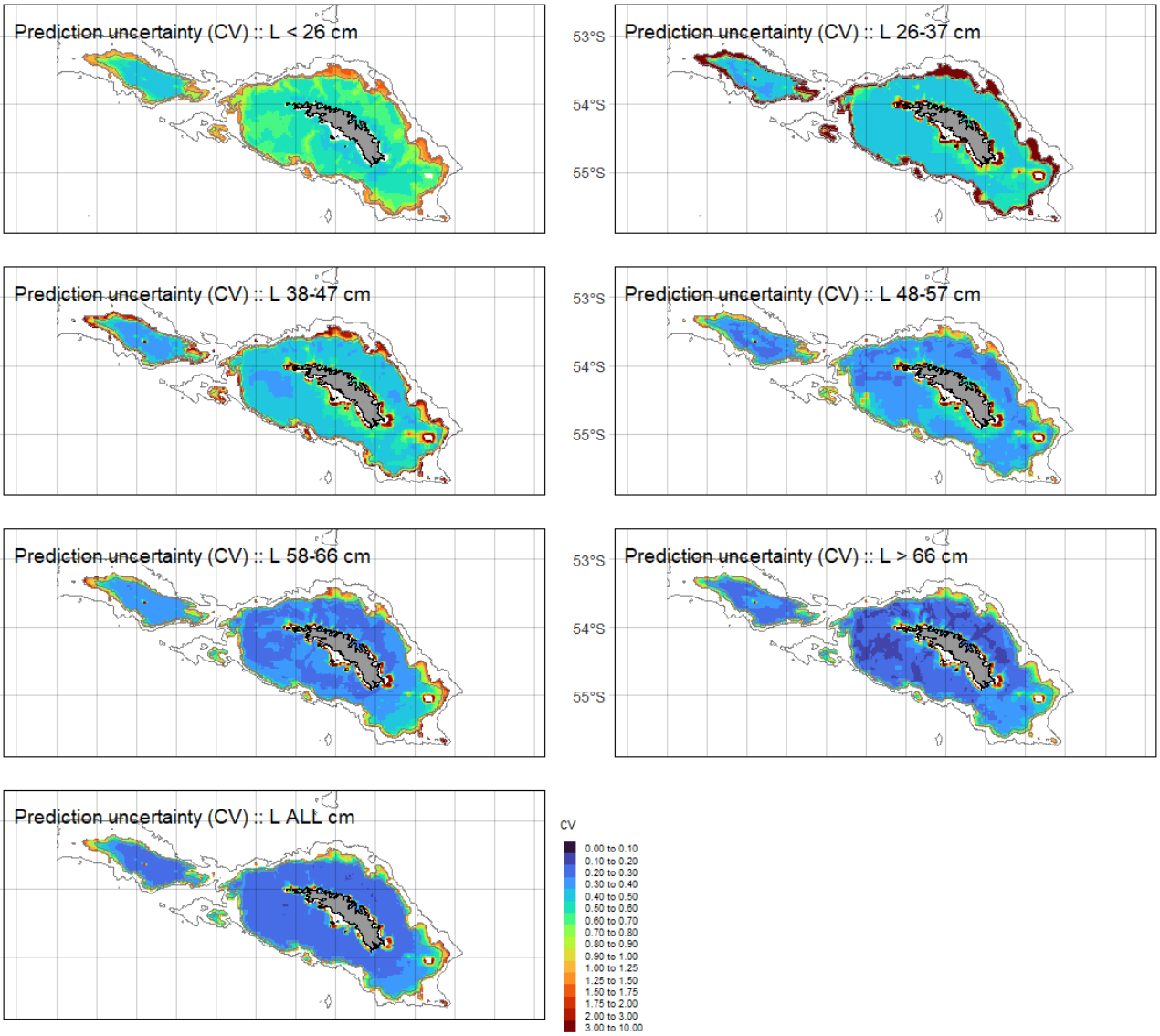

Figure S11. *Uncertainty of model-estimated Patagonian toothfish distribution around South Georgia and Shag Rocks. Values for uncertainty were calculated from the best predicting model for each size class as half the difference between the upper (mean + 1 SE) and lower (mean – 1SE) fitted density estimates (after transforming from the log-link scale) divided by the mean, to replicate a measure of uncertainty similar to coefficient of variation. Contours in each map panel correspond to the 500, 1000, and 2000 m isobaths. Values for locations shallower than 70 m and deeper than 1000 m are not shown as trawls included in our analyses were only performed at 70 – 920 m.*

Section 4: Additional results for longline analyses

Table S3. *Model results for analyses of longline CPUE data at South Georgia and the South Sandwich Islands. Models presented are the null model, containing vessel-year random effects, continuous trends through time, seasonal effects (day-of-year), lunar phase and soak time, with additions of depth, dynamic (SFT_dyn) or climatological (SFT_clim) seafloor temperature, and spatial variation. Statistics are the estimated degrees of freedom (EDF), Akaike's Information Criterion (AIC) and the difference in AIC relative to the best model.*

Model	EDF	AIC	ΔAIC
South Georgia			
NULL*	145.9	444432	1496
+ s(depth)	153.9	444208	1271
+ s(SFT_dyn)	154.6	444279	1343
+ s(SFT_clim)	153.1	444212	1276
+ s(east, north, bs='gp')	212.8	443076	140
+ s(depth) + s(SFT_dyn)	159.6	444161	1224
+ s(depth) + s(SFT_clim)	160.6	444143	1207
+ s(depth) + s(east, north, bs='gp')	219.5	442964	27
+ s(SFT_dyn) + s(east, north, bs='gp')	219.6	443064	127
+ s(SFT_clim) + s(east, north, bs='gp')	218.8	442987	50
+ s(depth) + s(SFT_dyn) + s(east, north, bs='gp')	223.4	442939	4
+ s(depth) + s(SFT_clim) + s(east, north, bs='gp')	**226.2**	**442936**	**0**
South Sandwich Islands (SSI)			
NULL*	42.4	16408	1887
+ s(depth)	45.6	16339	1819
+ s(SFT_dyn)	48.4	16259	1739
+ s(SFT_clim)	49.8	15681	1161
+ s(east, north, bs='gp')	70.6	14548	28
+ s(depth) + s(SFT_dyn)	53.8	16070	1549
+ s(depth) + s(SFT_clim)	53.1	15241	720
+ s(depth) + s(east, north, bs='gp')	73.0	14547	27
+ s(SFT_dyn) + s(east, north, bs='gp')	73.6	14547	27
+ s(SFT_clim) + s(east, north, bs='gp')	**76.1**	**14520**	**0**
+ s(depth) + s(SFT_dyn) + s(east, north, bs='gp')	78.0	14549	29
+ s(depth) + s(SFT_clim) + s(east, north, bs='gp')	76.5	14523	2

*: Null model = weight ~ offset(log(hooks)) + s(ship_year, bs= 're') + s(year) + s(day_of_year) + s(lunar) + s(soak_time)

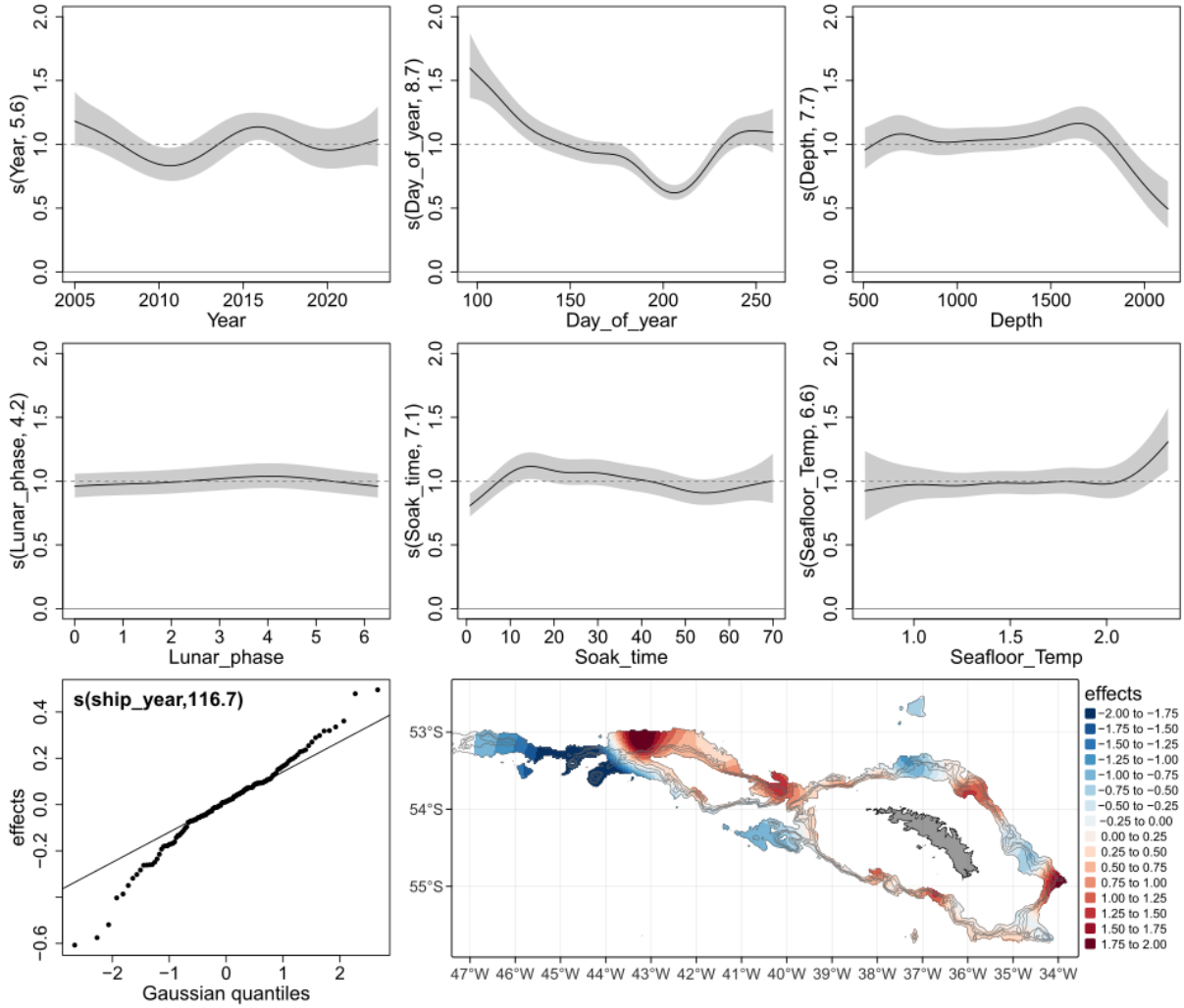

Figure S12. *Fitted relationships for CPUE estimated by fitting a Generalised Additive Model (GAM) to longline fishery catch data from South Georgia. Panels show the fitted variation in CPUE (holding all other variables constant) according to survey date (year), day of year, set depth (m), lunar phase, set duration (soak time; hours), seafloor temperature (°C), random effects of ship-year, and spatial variation. In each, CPUE is converted to a relative scale by dividing all values by the mean across the covariate range so that relationships are on the same scale to facilitate comparisons of effect size among covariates. With the exception of spatial and random effects, fitted relationships are shown as the mean ± 2 standard errors (shading).*

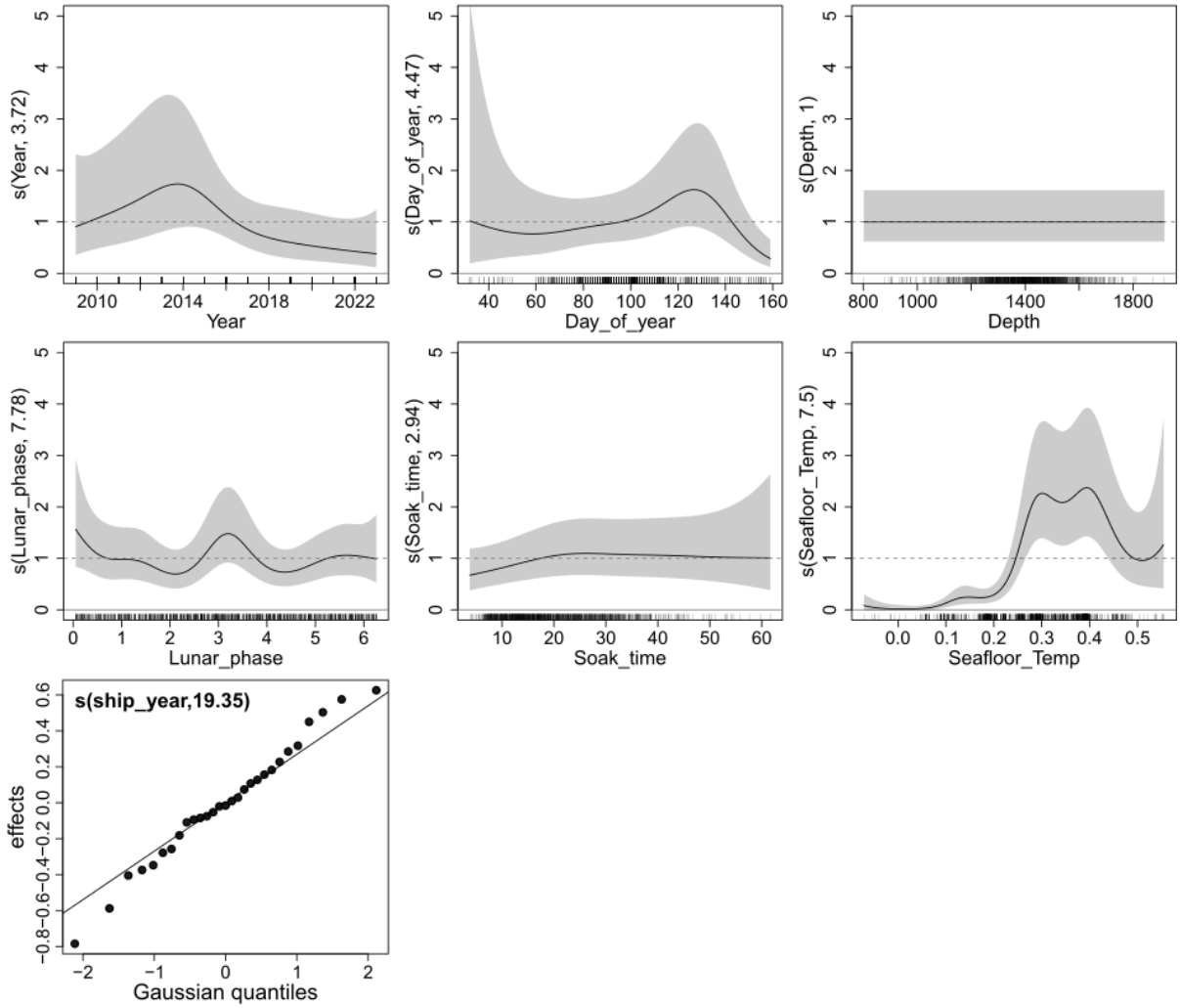

Figure S13. *Fitted relationships for CPUE estimated by fitting a Generalised Additive Model (GAM) without spatial effects to longline fishery catch data from the South Sandwich Islands. Panels show the fitted variation in CPUE (holding all other variables constant) according to survey date (year), day of year, set depth (m), lunar phase, set duration (soak time; hours), seafloor temperature (°C), and random effects of ship-year. In each, CPUE is converted to a relative scale by dividing all values by the mean across the covariate range so that relationships are on the same scale to facilitate comparisons of effect size among covariates. Excepting random effects, fitted relationships are shown as the mean ± 2 standard errors (shading).*

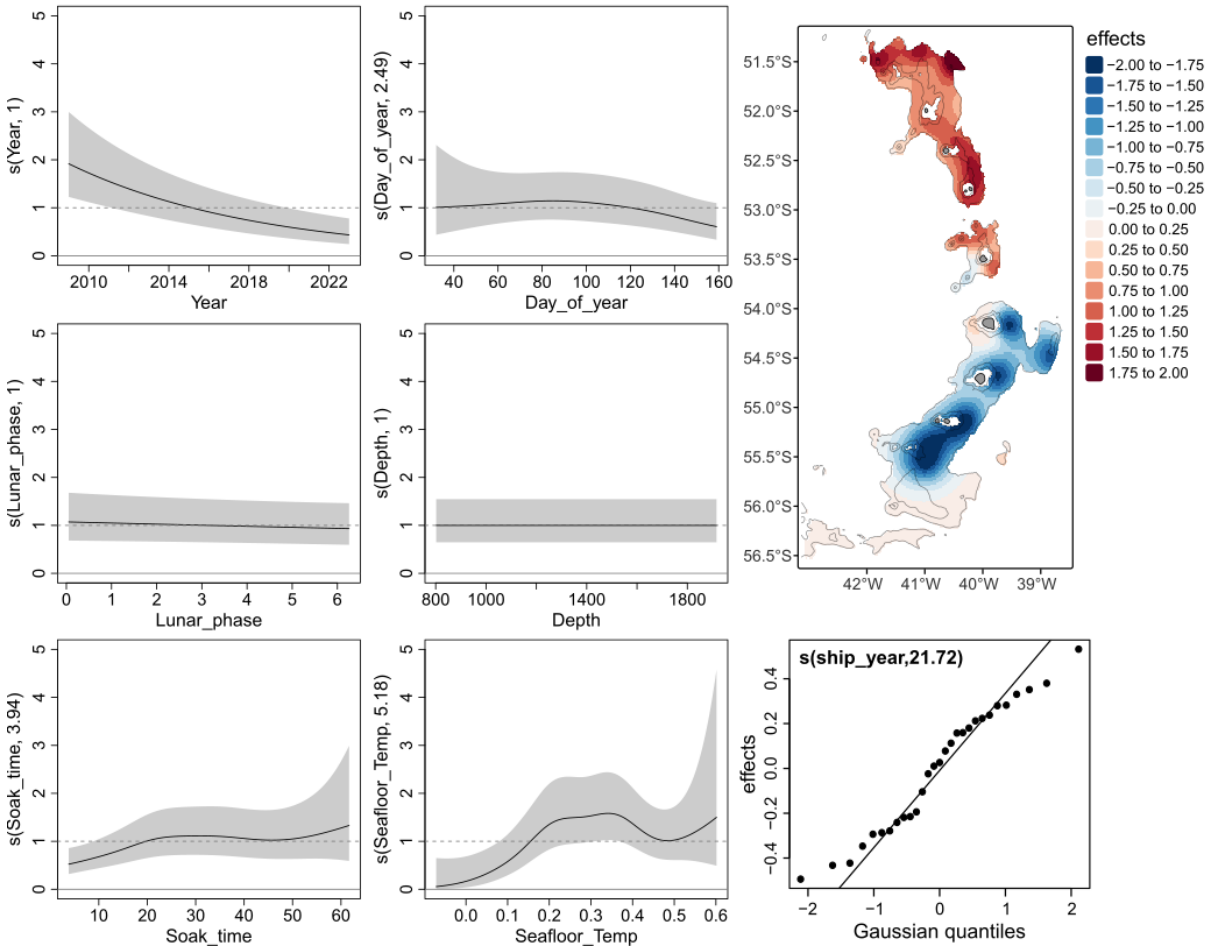

Figure S14. *Fitted relationships for CPUE estimated by fitting a Generalised Additive Model (GAM), inclusive of spatial fields, to longline fishery catch data from the South Sandwich Islands. Panels show the fitted variation in CPUE (holding all other variables constant) according to survey date (year), day of year, set depth (m), lunar phase, set duration (soak time; hours), seafloor temperature (°C), spatial variation, and random effects of ship-year. In each, CPUE is converted to a relative scale by dividing all values by the mean across the covariate range so that relationships are on the same scale to facilitate comparisons of effect size among covariates. With the exception of spatial and random effects, fitted relationships are shown as the mean ± 2 standard errors (shading).*

Section 5: Temperature trends across the Patagonian toothfish range

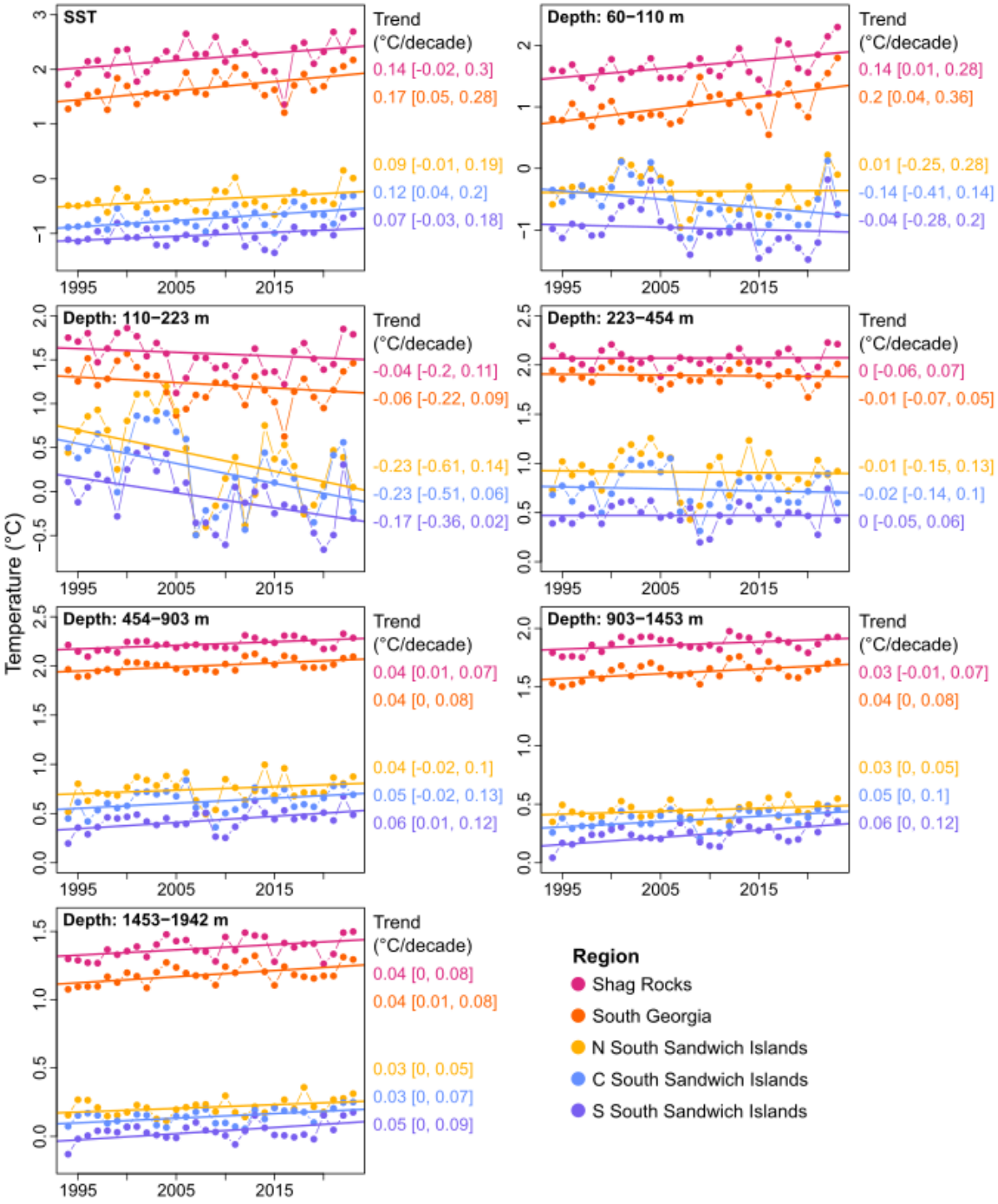

Figure S15. *Variation and trends in water temperature for different depth strata and regions throughout the known range of Patagonian toothfish in the Scotia Sea from 1994-2023. Values represent the year-average temperature within the 2000 m isobath for each region (Shag Rocks = 40-44°W, South Georgia = east of 40°W, N SSI = north of 57°S, C SSI = 57-58.1°S, S SSI = 58.2-60.5°S) at the stated depth range. All data were obtained from the Copernicus Marine Data Store, with sea surface temperature (SST) extracted from the Global Ocean OSTIA SST dataset, and remaining data extracted from the Global Ocean Physics Reanalysis dataset. Linear trend lines and trend estimates in °C/decade derive from a linear model fitted via gls with an AR1 correlation structure to account for temporal autocorrelation.*